# Lawrence Berkeley Laboratory
UNIVERSITY OF CALIFORNIA



## Materials & Molecular Research Division



Submitted to the Annual Reviews of Nuclear and Particle Science

# THE PARITY NON-CONSERVING ELECTRON-NUCLEON INTERACTION

E. D. Commins and P. H. Bucksbaum

January 1980



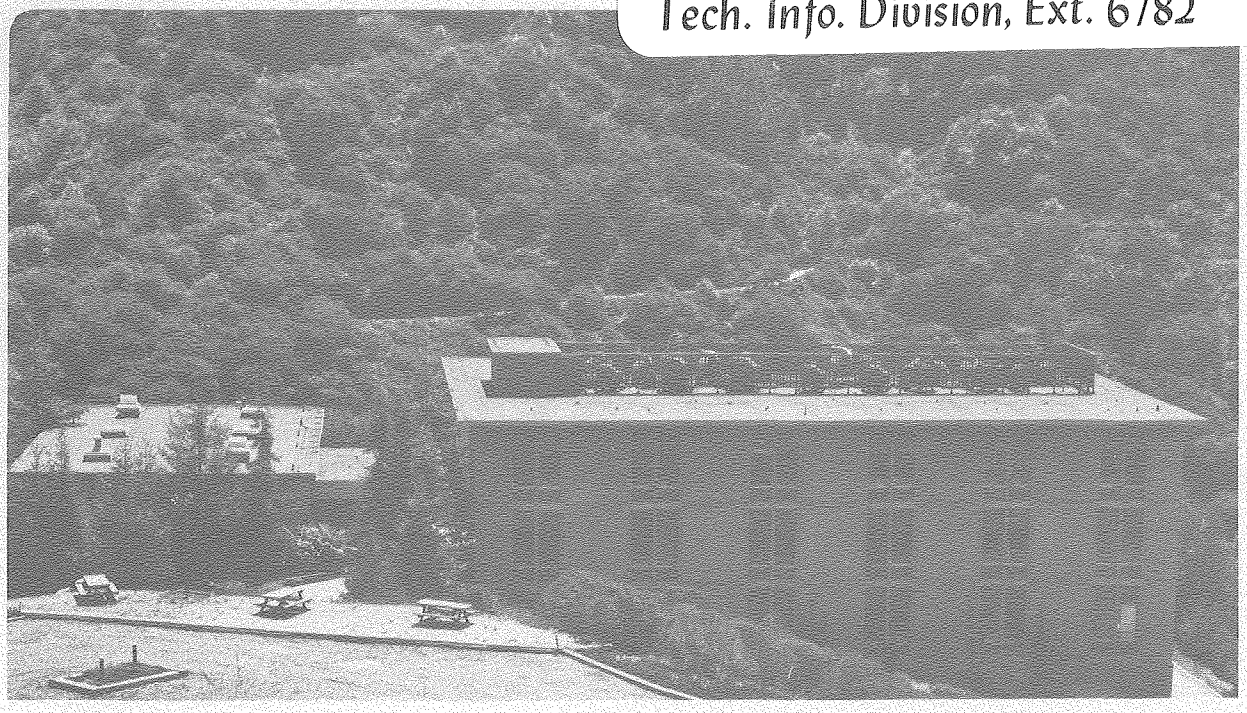

Prepared for the U.S. Department of Energy under Contract W-7405-ENG-48

## DISCLAIMER

LBL-10307

# THE PARITY NON-CONSERVING ELECTRON-NUCLEON INTERACTION

E.D. Commins and P.H. Bucksbaum
Department of Physics, University of California
and
Materials and Molecular Research Division, Lawrence Berkeley Laboratory
Berkeley, California 94720

Shortened Title: PARITY VIOLATION IN THE eN INTERACTION

Send Proofs to: Prof. Eugene D. Commins, Department of Physics,
University of California, Berkeley, CA 94720

CHAPTER HEADINGS

# 1. INTRODUCTION

It is now known that parity is violated in the electron-nucleon interaction $e + N \to e + N$. The results of diverse experiments, employing scattering of high energy polarized electrons and low energy atomic spectroscopy, imply that e and N (or in more basic terms e and quark q) engage in a neutral weak coupling, in addition to their much more powerful electromagnetic interaction. This neutral weak eq coupling now takes its place (see Table 1) with the observed neutral weak interactions $\nu q$ and $\nu e$, knowledge of which is by now quite extensive. Yet to be observed in their own right are the neutral weak couplings (ee) or (qq). Nevertheless the experimental facts from the $\nu q$, $\nu e$, and eq sectors are already sufficient to provide a stringent test of theoretical models, and the evidence is strongly in favor of the unified theory of weak and electromagnetic interaction proposed by Weinberg and Salam. In the remainder of this section we shall present general ideas concerning the neutral weak eq interaction. Then we shall describe the salient features of the Weinberg-Salam model (section 2), discuss in detail the principles and methods of the SLAC polarized electron scattering experiment (section 3) and atomic physics experiments (section 4), and summarize neutral weak interaction results and their implications (section 5).

Unlike the ($\nu q$) and ($\nu e$) interactions, the (eq) interaction is described by an amplitude containing an electromagnetic as well as a weak portion: $A = A_{EM} + A_W$, with $A_{EM} >> A_W$. In each (eq) process, the transition probability, proportional to $|A|^2$, thus contains an interference term $\sim 2A_W A_{EM}$ in addition to the dominant term $|A_{EM}|^2$ and the

very small term $|A_W|^2$ (which we neglect). If the weak interaction violates parity, the interference term contains a pseudoscalar portion $A_{WP}$, the sign of which depends on the "handedness" of the coordinate system in which the experiment is performed. When the rates for a process $I_\pm$ in the two coordinate frames of opposite handedness are compared, one obtains an asymmetry

$$\Delta = \frac{I_+ - I_-}{I_+ + I_-} \sim \frac{A_{WP}}{A_{EM}} . \qquad (1)$$

In the case of high-energy electron scattering at SLAC the handedness is defined by the helicity of the longitudinally polarized electron beam. We may estimate $\Delta$ crudely in this case by employing the Feynman diagrams for the electromagnetic and neutral weak interactions in lowest order (Figure 1).[1] The former proceeds by photon exchange, with $A_{EM} = 4\pi\alpha/q^2$.

The latter is presumed to be mediated by a neutral vector boson $Z_o$. Even in primitive theories which attempt to establish a connection between weak and electromagnetic interactions its mass should be $m_Z \sim (\pi\alpha/G)^{\frac{1}{2}}$. For $|q^2| << m_Z^2$ the weak amplitude should be of order G. Assuming that parity is violated near-maximally for the neutral weak interactions as it is for charged weak interactions, we find:

---

[1] We adhere to the relativistic conventions employed by Bjorken & Drell (1964); q is the invariant four momentum transfer from electron to nucleon, and $q^2 < 0$ for spacelike q . Also $\alpha = e^2/4\pi\hbar c \simeq 1/137$, we employ units $\hbar = c = 1$ unless otherwise noted, and the Fermi coupling constant is $G = 1.02 \times 10^{-5}\ m_p^{-2}$, where $m_p$ is the proton mass.

$$\Delta = \frac{\sigma_+ - \sigma_-}{\sigma_+ + \sigma_-}$$

$$\sim A_W/A_{EM}$$

$$\sim Gq^2/4\pi\alpha \sim q^2/m_Z^2. \qquad (2)$$

For $|q^2| \approx (1\ \text{GeV})^2$ this yields $\Delta \approx 10^{-4}$, an estimate originally given by Zel'dovich (1959). According to a more detailed analysis presented in section 3, the electron scatters from individual quark-partons in the nucleus (Cahn & Gilman 1978). The weak and electromagnetic contributions from each quark are coherent and interfere, but the sum over all quarks is incoherent. The asymmetry predicted on the basis of the Weinberg-Salam model, and actually obtained in the experiment (Prescott et al 1978, 1979) is still of order $10^{-4}$.

One employs the same amplitudes (Figure 1) in low energy atomic physics, but they are described in somewhat different language. Photon exchange between atomic electron and nucleus is expressed by the ordinary atomic Hamitonian $H_o$, whose eigenstates, the usual atomic states, may be separated into two classes $|\psi_n^o\rangle$, $|\chi_m^o\rangle$ of opposite parity. Exchange of the massive $Z^o$ is described by an effective zero-range potential H' of order G, which contains scalar and pseudoscalar parts: $H' = H_S + H_P$ (Bouchiat & Bouchiat 1974a,b, 1975). $H_S$ is in principle observable (it leads to energy shifts), but these are so small that they cannot be separated from effects due to $H_o$ in any known practical experiment, because of small uncertainties in $H_o$. $H_P$ is a significant perturbation on $H_o$, however, since it causes a state $|\psi^o\rangle$ to be admixed with states $|\chi^o\rangle$ of opposite parity:

$$|\psi^o\rangle \rightarrow |\psi\rangle = |\psi^o\rangle + \sum_n \frac{|\chi_n^o\rangle\langle\chi_n^o|H_p|\psi^o\rangle}{E(\psi^o) - E(\chi_n^o)} \,. \qquad (3)$$

Let us consider how the electronic and nucleonic currents contribute to the pseudoscalar portion of the Hamiltonian $H_p$. A priori these currents may possess scalar (S), vector (V), tensor (T), axial vector (A) and pseudoscalar (P) components. Thus, neglecting momentum transfer dependent terms we may write

$$H_P = \sum_{V,A,S,P,T} Gc_k (\bar{\psi}_N \Gamma_k \psi_N)(\bar{\psi}_e \Gamma_k \gamma_5 \psi_e)$$

where the $c_k$ are coefficients to be determined. However, the term corresponding to $\Gamma_k = \gamma_5$ (P term) vanishes in the non-relativistic nucleon limit. Also it can be shown that the S and T terms are time reversal odd as well and lead to a permanent electric dipole moment of the atom (Hinds 1976, Sandars 1968). Experiments to search for linear Stark effect in Xe, Cs, and Tℓ place an upper limit on the coefficients $c_S$, $c_T$ of less than $10^{-3}$ (Hinds 1976, Player & Sandars 1970, Bouchiat 1975, Gould 1970). Furthermore, it can be shown that the S, T, and P terms yield no interference with electromagnetism in high energy electron scattering where quark and electron masses may be neglected. Thus, we shall assume that the electronic and nucleonic weak neutral currents contain only vector and axial vector components:

$$J_e = V_e + A_e$$

$$J_N = V_N + A_N.$$

Then, we may write $H_p = H_p^{(1)} + H_p^{(2)}$, where $H_p^{(1)}$, $H_p^{(2)}$ arise from the combinations $A_e V_N$ and $V_e A_N$, respectively. Ignoring momentum transfer-dependent terms, we have:

$$H_p^{(1)} = \frac{G}{\sqrt{2}} \sum_i \bar{\psi}_e \gamma_\lambda \gamma_5 \psi_e [C_{1p} \bar{\psi}_{pi} \gamma^\lambda \psi_{pi} + C_{1n} \bar{\psi}_{ni} \gamma^\lambda \psi_{ni}] \qquad (4)$$

$$H_p^{(2)} = \frac{G}{\sqrt{2}} \sum_i \bar{\psi}_e \gamma_\lambda \psi_e [C_{2p} \bar{\psi}_{pi} \gamma^\lambda \gamma_5 \psi_{pi} + C_{2n} \bar{\psi}_{ni} \gamma^\lambda \gamma_5 \psi_{ni}] \qquad (5)$$

where the sum is taken over all protons (p) and neutrons (n) in the nucleus.

The coupling coefficients $C_{1p}$, $C_{1n}$, $C_{2p}$, $C_{2n}$ are model-dependent and must be determined by experiment. As will be demonstrated in Section 2, the Weinberg-Salam model (Weinberg 1967, Salam 1968) predicts:

$$C_{1p} = \tfrac{1}{2}(1 - 4 \sin^2\theta) \qquad (6a)$$

$$C_{1n} = -\tfrac{1}{2} \qquad (6b)$$

$$C_{2p} = \frac{g_A}{2} (1 - 4 \sin^2\theta) \qquad (6c)$$

$$C_{2n} = -\frac{g_A}{2} (1 - 4 \sin^2\theta) \qquad (6d)$$

where $g_A = 1.25$ is the axial vector coupling constant of neutron beta decay, and $\theta$ is the Weinberg angle (Weinberg 1972). A variety of experiments yield $\sin^2\theta = 0.23$. Assuming Eqs. (6) and performing a non-relativistic reduction of the nucleonic currents we obtain from Eq. (4) the effective electronic weak Hamiltonian corresponding to $A_e V_N$:

$$H_W^{(1)} = \frac{G}{2\sqrt{2}} Q_W \rho_N(\vec{r}) \gamma_5 \tag{7}$$

where $Q_W = (1 - 4 \sin^2\theta)Z - N$ and $\rho_N(\vec{r})$ is the nuclear density, $\vec{r}$ being the electron position. In the limit of a point nucleus and a non-relativistic electron, Eq. (7) yields:

$$H_W^{(1)} \to \frac{G}{4\sqrt{2}} \frac{1}{m_e c} Q_W [\vec{\sigma}\cdot\vec{p}\delta^3(\vec{r}) + \delta^3(\vec{r})\vec{\sigma}\cdot\vec{p}] \tag{8}$$

where $\vec{\sigma},\vec{p}$ refer to the electron. In the first (second) term on the RHS of Eq. (8), $p = -i\hbar\vec{\nabla}$ is understood to apply to the electronic wave function on the left(right) in $\langle\chi|H_W^{(1)}|\psi\rangle$. The factor $Q_W \sim Z$ arises because we sum coherently over each nucleon (since the atomic electron wavelength is much larger than the nuclear diameter).

In the case of $H_p^{(2)}$ which corresponds to $V_e A_N$, a non-relativistic reduction of the axial nucleonic current yields factors proportional to nucleon spin, and these cancel in pairs in the sum over nucleons, leaving at most two unpaired spins. Thus in the non-relativistic limit of the electron and for a point nucleus, the Weinberg-Salam model yields an effective Hamiltonian:

$$H_W^{(2)} = \frac{G}{4\sqrt{2}} \frac{1}{m_e c} (1 - 4 \sin^2\theta) g_A \vec{\sigma}_N\cdot\vec{\sigma}[\vec{\sigma}\cdot\vec{p}\delta^3(\vec{r}) + \delta^3(\vec{r})\vec{\sigma}\cdot\vec{p}]. \tag{9}$$

$H_W^{(2)}$ contains no enhancement factor $Q_W$ and its effects are therefore smaller than those of $H_W^{(1)}$ by a factor $\sim Z(1 - 4 \sin^2\theta)^{-1}$. $H_W^{(2)}$ is therefore quite negligible compared to $H_W^{(1)}$ for heavy atoms where $Z >> 1$.

We now consider an electromagnetic transition between two atomic states $|\psi_1\rangle$, $|\psi_2\rangle$ of the same nominal parity (i.e., absorption or emission of an optical or microwave magnetic dipole photon). Examples

would be the transitions $1^2S_{\frac{1}{2}} \to 2^2S_{\frac{1}{2}}$ in H, $6^2P_{\frac{1}{2}} \to 7^2P_{\frac{1}{2}}$ in Tℓ. From Eq. (3), the transition amplitude is, to order G:

$$\langle\psi_2|O_{EM}|\psi_1\rangle \simeq \langle\psi_2^o|O_{EM}|\psi_1^o\rangle + \mathcal{E}_p \tag{10}$$

where the first term on the RHS is the zero-order M1 amplitude $\mathcal{M}$ and $\mathcal{E}_p$, given by

$$\mathcal{E}_p = \sum_n \left\{ \frac{\langle\psi_2^o|O_{EM}|\chi_n^o\rangle\langle\chi_n^o|H_p|\psi_1^o\rangle}{E(\psi_1^o) - E(\chi_n^o)} + \frac{\langle\psi_2^o|H_p|\chi_n^o\rangle\langle\chi_n^o|O_{EM}|\psi_1^o\rangle}{E(\psi_2^o) - E(\chi_n^o)} \right\}, \tag{11}$$

is an electric dipole (E1) amplitude caused by parity violation. In a standard phase convention $\mathcal{M}$ is real; then from Eqs. (8) or (9), $\mathcal{E}_p$ is imaginary, and in general this is required by time reversal (T) invariance.

Experiments have been proposed to detect the existence of $\mathcal{E}_p$ in the isotopes of atomic hydrogen, and in heavy atoms (Cs, Tℓ, Bi). So far parity violation has been observed in Tℓ and Bi. The hydrogenic atom experiments are important because the electronic wave-functions are known exactly, so no uncertainty is introduced by atomic theory, and in principle one can measure all four coupling constants $C_{1p}$, $C_{1n}$, $C_{2p}$, $C_{2n}$. However, the expected effects are small and very difficult to observe. In heavy atoms the effects are larger than in hydrogen but uncertainties in atomic theory make precise calculations of $\mathcal{E}_p$ a difficult task. Moreover, since $H_W^{(1)}$ greatly dominates over $H_W^{(2)}$ for large Z, only the coefficients $C_{1p}$ and $C_{1n}$ can be studied. Indeed, in the Weinberg-Salam model, with $\sin^2\theta = 0.23$, the contribution of $C_{1p}$ is much less than that of $C_{1n}$.

## 2. THE WEINBERG-SALAM MODEL

### 2.1 Local Gauge Invariance

The unified theory of weak and electromagnetic interactions is based on the principle of local gauge invariance, according to which the Lagrangian density describing the various particles and their interactions must be invariant under a local gauge transformation; that is, one which can vary in an arbitrary manner from one space-time point to another. The Dirac Lagrangian density for a free electron:

$$\mathcal{L}_D = \tfrac{1}{2}\bar{\psi}(i\gamma^\mu\partial_\mu - m)\psi - \tfrac{1}{2}[i(\partial_\mu\bar{\psi})\gamma^\mu + m\bar{\psi}]\psi \qquad (12)$$

is invariant under the infinitesimal global U(1) gauge transformation $\delta\psi = \psi' - \psi = i\beta\psi$ ($\beta$ an infinitesimal real constant). However, under the local U(1) gauge transformation $\delta\psi = i\alpha(x_\mu)\psi$ ($\alpha$ a real infinitesimal depending on the $x_\mu$), $\mathcal{L}_D$ is not invariant. In fact, $\delta\mathcal{L}_D = \mathcal{L}_D' - \mathcal{L}_D = -(\partial_\mu\alpha)\cdot\psi\gamma^\mu\psi$. Nevertheless, the invariance is restored by adding to $\mathcal{L}_D$ the term:

$$\mathcal{L}_I = -g'\bar{\psi}\gamma^\mu\psi \cdot B_\mu \qquad (13)$$

where $g'$ is a constant, and $B_\mu$ is a vector field, provided we stipulate that under the gauge transformation,

$$\delta B_\mu(x) = B'_\mu(x) - B_\mu(x) = -\frac{1}{g'}\partial_\mu\alpha. \qquad (14)$$

The addition of $\mathcal{L}_I$ to $\mathcal{L}_D$ is equivalent to the replacement of the ordinary derivative by the "covariant" derivative $\partial_\mu \to \nabla_\mu \equiv \partial_\mu + ig'B_\mu$ in $\mathcal{L}_D$. If we were to put $g' = e$ and identify $B_\mu$ as the ordinary vector potential $A_\mu$, Eq. (14) would become the familiar gauge transformation condition of electrodynamics. $\mathcal{L}_I$ in Eq. (13) would then be the "minimal"

interaction Lagrangian, seen here to arise from the condition of local gauge invariance. Of course, in electrodynamics it is necessary to include an additional gauge invariant term corresponding to the field alone:

$$\mathcal{L}_{EM} = -\tfrac{1}{4}F_{\mu\nu}F^{\mu\nu} \tag{15}$$

where

$$F_{\mu\nu} = \partial_\mu A_\nu - \partial_\nu A_\mu. \tag{16}$$

These ideas are readily extended to the case of an isodoublet "Yang-Mills" field $\psi = \begin{pmatrix}\psi_1\\ \psi_2\end{pmatrix}$ (Yang & Mills 1954). We consider the local SU(2) gauge transformation:

$$\delta\psi = \psi' - \psi = i\varepsilon^i\left(\frac{\tau_i}{2}\right)\psi \equiv i\hat{\varepsilon}\psi \tag{17}$$

where the $\tau^i$ (i = 1,2,3) are 2×2 Pauli matrices, and the real infinitesimals $\varepsilon_i$ depend on the $x_\mu$. Defining a Lagrangian $\mathcal{L}_D$ for the doublet $\psi$ as in Eq. (12) we find

$$\delta\mathcal{L}_D = -\bar{\psi}\gamma^\mu(\partial_\mu\hat{\varepsilon})\psi. \tag{18}$$

Now defining a triplet of vector fields $\vec{A} = A_\mu^{1,2,3}$ and $\hat{A}_\mu \equiv A_\mu^i(\tau_i/2)$, we restore the invariance of $\mathcal{L}_D$ by making the replacement $\partial_\mu \to \nabla_\mu = \partial_\mu + ig\hat{A}_\mu$ (g a constant), provided that

$$\partial\hat{A}_\mu = -\frac{1}{g}\partial_\mu\hat{\varepsilon} + i[\hat{\varepsilon},\hat{A}_\mu]. \tag{19}$$

A term analogous to that in Eq. (15) must be added to describe the "field energy"

$$\mathcal{L}_{YM} = -\tfrac{1}{4}f_{\mu\nu}f^{\mu\nu}, \tag{20}$$

but now, since $\hat{A}_\mu, \hat{A}_\nu$ are 2×2 matrices, in general non-commuting, we require

$$f_{\mu\nu} = \partial_\mu \hat{A}_\nu - \partial_\nu \hat{A}_\mu + ig[\hat{A}_\mu, \hat{A}_\nu] \qquad (21)$$

in order that $\mathcal{L}_{YM}$ shall be gauge-invariant. The term in Eq. (21) proportional to g has no analog in electrodynamics. Physically it corresponds to the fact that the fields $A_\mu^{1\pm i2}$ themselves carry "charge," and it implies that nonlinear self-interaction terms of order g ("$A^3$") and $g^2$ ("$A^4$") appear in Eq. (20).

When the fields $\vec{A}_\mu$ and $\vec{B}_\mu$ are quantized,[1] four massless vector quanta appear; two neutral: $(A_\mu^3, B_\mu)$, and two charged: $(1/\sqrt{2})(A_\mu^{1\pm i2})$. Attractive possibilities are thus suggested for a unified theory of weak interactions (charged and neutral), and electromagnetic interactions (neutral), in which vector fermion currents are coupled to the aforementioned vector fields. However, at this stage the theory is still unacceptable, for several reasons. First, weak currents have axial-vector as well as vector components. This requires that $\mathcal{L}_D$ also be invariant under chiral gauge transformations $\delta\psi = i\eta^i(\tau_i/2)\gamma^5\psi$, where the $\eta^i$ are real infinitesimals depending on the $x_\mu$. It can easily be shown that this requires $m_{fermion} = 0$ in $\mathcal{L}_D$, and an additional means must therefore be found to give mass to the fermions without spoiling gauge invariance. Second, the weak interactions are short-ranged, and thus at least some of the Yang-Mills quanta must gain mass, without spoiling the local gauge invariance or renormalizablity, another attractive feature of the massless theory.

## 2.2 Spontaneous Symmetry Breaking

The problem of massive gauge quanta is solved by means of "spontaneous symmetry breaking," a crucial feature added to the SU(2)×U(1)

[1] See, for example, Abers & Lee, (1973).

Yang-Mills theory by Weinberg (1967) and Salam (1968). Spontaneous symmetry breaking refers to the situation in which a Lagrangian possesses a symmetry not shared by the ground state of the system. In field theories not of the gauge (Yang-Mills) type, it can be shown (Goldstone 1961, Goldstone et al 1962) that there is massless spin-zero excitation (the so-called "Goldstone boson") for each degree of freedom in which the symmetry is spontaneously broken. However, the proof of this statement is based on two assumptions: manifest covariance and a positive metric in Hilbert space. In a gauge theory, one or the other of these conditions is always invalid. The net effect in the case of a Yang-Mills field is that the Goldstone theorem is evaded [the Higgs phenomenon, see Higgs (1964a,b, 1966), Englert & Brout (1964), Guralnik et al (1964)], each of the unwanted Goldstone bosons disappears, and in its place a corresponding massive gauge field appears. In this process, renormalizability is retained, as was first proved by 't. Hooft. [See 't. Hooft (1971), Lee (1972a,b), Abers & Lee (1973)]. In an oft-quoted example, we may consider a complex scalar isodoublet (charged)field

$$\phi = \begin{pmatrix} \dfrac{\phi_1 + i\phi_2}{\sqrt{2}} \\ \dfrac{\phi_3 + i\phi_4}{\sqrt{2}} \end{pmatrix}$$

where $\phi_1, \ldots \phi_4$ are real scalar fields. We employ the SU(2)×U(1) globally-invariant langrangian density:

$$= (\partial_\mu \phi^\dagger)(\partial^\mu \phi) - \mu^2 \phi^\dagger \phi - \lambda (\phi^\dagger \phi)^2 \qquad (22)$$

where $\mu^2 > 0$ and $\lambda > 0$ correspond to mass ($\phi^2$) and "$\phi^4$" interaction terms, respectively. We now regard $\mu^2$ as a variable parameter. For $\mu^2 > 0$,

Eq. (22) describes four real scalar fields with the same mass, and also the vacuum state of the system (classically, the state with lowest energy) is $\phi = 0$. However, for $\mu^2 < 0$ the symmetry of the ground state is broken; the lowest energy state is not $\phi = 0$, and one obtains three scalar fields with zero mass (these correspond to Goldstone bosons) and one scalar field with finite mass $\sqrt{-2\mu^2}$.

However, let us now require $\mathcal{L}$ in Eq. (22) to be rendered invariant under <u>local</u> SU(2)×U(1) gauge transformations, by the replacement

$$\partial_\mu \to \nabla_\mu \equiv (\partial_\mu + ig\hat{A}_\mu + \frac{ig'}{2} B_\mu I) \tag{23}$$

where I is the 2×2 identity matrix. The constants g and g', corresponding to SU(2) and U(1) gauge transformations respectively, are independent. We also add to Eq. (22) the terms $-\frac{1}{4}f_{\mu\nu}f^{\mu\nu} - \frac{1}{4}G_{\mu\nu}G^{\mu\nu}$, where $f_{\mu\nu}$ is defined in Eq. (21), and

$$G_{\mu\nu} = \partial_\mu B_\nu - \partial_\nu B_\mu. \tag{24}$$

We make the substitutions

$$\eta^2 \equiv -\mu^2/2\lambda \quad (\eta^2 > 0 \text{ for } \mu^2 < 0)$$

$$g'/g \equiv \tan\theta$$

and define the new vector fields:

$$Z_\mu = \cos\theta\, A_\mu^3 - \sin\theta\, B_\mu \tag{25a}$$

$$A_\mu = \sin\theta\, A_\mu^3 + \cos\theta\, B_\mu \tag{25b}$$

where $A_\mu$ is a new field, not to be confused with $\vec{A}_\mu$. In a straightforward analysis in which higher order infinitesimals are dropped, the modified Lagrangian becomes

$$\mathcal{L} = [\tfrac{1}{2}(\partial_\mu\sigma)(\partial^\mu\sigma) - \tfrac{1}{2}(-2\mu^2)\sigma^2]$$

$$-\tfrac{1}{4}Z_{\mu\nu}Z^{\mu\nu} + \tfrac{1}{2}\frac{g^2\eta^2}{2\cos^2\theta}Z_\mu Z^\mu$$

$$-\tfrac{1}{4}[A_{\mu\nu}A^{\mu\nu} + A^2_{\mu\nu}A^{2,\mu\nu}]$$

$$+\tfrac{1}{2}\frac{g^2\eta^2}{2}[A_\mu A^\mu + A^2_\mu A^{2\mu}]$$

$$-\tfrac{1}{4}A_{\mu\nu}A^{\mu\nu}. \qquad (26)$$

Here $Z_{\mu\nu} \equiv \partial_\mu Z_\nu - \partial_\nu Z_\mu$, etc. The first term in square brackets on the RHS of Eq. (26) corresponds to the kinetic energy and finite mass of the single scalar boson ("Higgs" boson). Such objects must necessarily arise in the procedure of spontaneous symmetry breaking even if a somewhat different choice is made for $\mathcal{L}$ in Eq. (22). The second and third terms correspond to the field energy and finite mass $m_Z^2 = g^2\eta^2/(2\cos^2\theta)$ of a neutral vector gauge boson $Z^o$. The fourth and fifth terms correspond to the field energy and finite mass $m_W^2 = g^2\eta^2/2$ of charged vector gauge bosons $W^\pm = (1/\sqrt{2})(A_\mu \mp iA^2_\mu)$. Finally the last term corresponds to the field energy of a massless vector field $A_\mu$, which we naturally identify as the EM field. Then using Eqs. (25a,b) the term $(g/2)A^3_\mu\tau_3 + (g'/2)B_\mu I$ in Eq. (23) can be rewritten:

$$\frac{g}{2}A^3_\mu\tau_3 + \frac{g'}{2}B_\mu I = A_\mu g\sin\theta\left(\frac{I+\tau_3}{2}\right) + Z_\mu g\cos\theta\left(\frac{\tau_3 - \tan^2\theta\cdot I}{2}\right). \qquad (27)$$

The first term on the RHS of Eq. (27) contains $A_\mu$ and the charge operator $\frac{1}{2}(I + \tau_3)$. Therefore, we can identify $g\sin\theta$ as the electric charge:

$$g\sin\theta = e. \qquad (28)$$

## 2.3 Coupling of Gauge Fields to Leptons and Quarks

We now introduce the material particles (leptons and quarks) and couple them to the gauge fields. Our choices here are largely constrained by the requirement that the new theory reproduce the known and valid results of electrodynamics and of the old "current-current" charged weak-interaction theory [Feynman & Gell-Mann (1958), Sudarshan & Marshak (1958)]. The charged weak interactions involve only the left-handed fields $e_L = \frac{1}{2}(1 - \gamma_5)e$, $\mu_L = \frac{1}{2}(1 - \gamma_5)$ , $u_L = \frac{1}{2}(1 - \gamma_5)u$, etc. Many experimental facts suggest the arrangement of all fermions in "weak left-handed isodoublets"(Glashow et al 1970):

$$\binom{\nu_e}{e}_L , \binom{\nu_\mu}{\mu}_L , \binom{\nu_\tau}{\tau}_L , \ldots \quad \text{(Leptons)}$$

$$\binom{u}{d_C}_L , \binom{c}{s_C}_L , \ldots \quad \text{(Quarks)}$$

where $d_C = d \cos\theta_C + s \sin\theta_C$, $s_C = -d \sin\theta_C + s \cos\theta_C$, $\theta_C$ is the Cabibbo angle, and u,d,s,c are the up, down, strange, and charged quarks. The right-handed fields $e_R = \frac{1}{2}(1 + \gamma_5)e$, $\mu_R = \frac{1}{2}(1 + \gamma_5)\mu$, etc., do not participate in any known way in the charged weak interaction, and this provides a clue as to their weak isomultiplet assignments. In the Weinberg-Salam model one assumes that the components $e_R, \mu_R, \ldots u_R, d_R, \ldots$ are all (right-handed) weak <u>isosinglets</u> under SU(2). Within SU(2)×U(1) other possibilities may be entertained but as we shall see, these are now ruled out by experiment.

It remains to determine the transformation properties of the fermions under U(1) from the electromagnetic couplings. We introduce the "weak hypercharge" Y, defined by the U(1) gauge transformation $\delta\chi = (i\alpha/2)(Y\chi)$ where $\alpha$ is a real infinitesimal depending on the $x_\mu$, $\chi$ is a column matrix

of the fermion fields:

$$\chi = \begin{pmatrix} \nu_{eL} \\ e_L \\ \nu_{eR} \\ e_R \\ \cdots \\ u_L \\ d_{cL} \\ u_R \\ d_R \\ \cdots \end{pmatrix} \begin{matrix} \} \text{ Leptons} \\ \\ \\ \\ \\ \} \text{ Quarks} \\ \\ \\ \\ \end{matrix}$$

and Y is an N N diagonal matrix. When the SU(2)×U(1) covariant derivative is introduced into the fermion Dirac langrangian, and if we assume the Weinberg-Salam weak isomultiplet structure, a minimal interaction coupling term arises, of the form:

$$\mathcal{L}_{INT} = -\bar{\chi}\gamma^{\mu}[gA_{\mu 1}L^1 + gA_{\mu 2}L^2 + gA_{\mu 3}L^3 + \tfrac{1}{2}g'B_{\mu}Y]\chi \qquad (29)$$

where $L^i = [(1 - \gamma_5)/2](\tau^i/2)$. Froms Eqs. (25) and (28) we find:

$$gA_{\mu 3}L^3 + \tfrac{1}{2}g'B_{\mu}Y = e(L^3 + \frac{Y}{2})A_{\mu} + g\cos\theta\,(L^3 - \frac{Y}{2}\tan^2\theta)Z_{\mu}. \qquad (30)$$

The first term on the RHS of Eq. (30) represents the EM coupling of each fermion; therefore $L^3 + (Y/2)$ is plainly the charge operator Q. The second term on the RHS of Eq. (30) may then be expressed in terms of $L^3$ and Q as $(g/\cos\theta)Z_{\mu}[L^3 - \sin^2\theta\, Q]$ which yields directly the neutral weak coupling of each fermion in terms of $L^3$ and Q.

To summarize, we write:

$$\mathcal{L}_{INT} = \mathcal{L}_{EM} + \mathcal{L}_C + \mathcal{L}_N \qquad (31)$$

for EM, charged weak, and neutral weak interactions respectively. Here $\mathcal{L}_{EM} = -eJ^{\lambda}_{EM}A_{\lambda}$, where:

$$J^{\lambda}_{EM} = \bar{\chi}\gamma^{\lambda}Q\chi. \qquad (32)$$

Next,

$$\mathcal{L}_C = -\frac{g}{2\sqrt{2}}\left(J_C^{\lambda+}W_\lambda^+ + J_C^{\lambda-}W_\lambda^-\right) \tag{33}$$

where $W_\lambda^\pm = (1/\sqrt{2})A^{1\pm i2}$,

$$J_C^{\lambda\pm} = \bar{\chi}\gamma^\lambda(1-\gamma_5)\frac{\tau^\pm}{2}\chi, \tag{34}$$

and $\tau^\pm = \tau_x \pm i\tau_y$. Finally, for the neutral weak interaction:

$$\mathcal{L}_N = -\frac{g}{2\cos\theta}J_N^\lambda Z_\lambda \tag{35}$$

where

$$J_N^\lambda = \bar{\chi}\gamma^\lambda(1-\gamma_5)\frac{\tau_3}{2}\chi - 2\sin^2\theta\, J_{EM}^\lambda. \tag{36}$$

We remind the reader that the $\tau_i$ refer to <u>weak</u> isospin. The constant g may be expressed in terms of the more familiar Fermi coupling constant G by comparing expressions for the muon decay amplitude in the new theory and in the old V-A theory. As is well known, the latter describes muon decay accurately in terms of the amplitude:

$$\mathcal{a} = \frac{G}{\sqrt{2}}u_{\nu_\mu}\gamma_\lambda(1-\gamma_5)u_\mu \cdot \bar{u}_e\gamma^\lambda(1-\gamma_5)v_{\bar{\nu}_e} \tag{37}$$

where the u's and v are single-particle Dirac spinors. From Eqs. (33) and (34), the new theory yields:

$$\mathcal{a} = -\frac{g^2}{8}\bar{u}_{\nu_\mu}\gamma_\lambda(1-\gamma_5)u_\mu \cdot \left[\frac{g^{\lambda\sigma} - q^\lambda q^\sigma/m_W^2}{q^2 - m_W^2}\right]\bar{u}_e\gamma_\sigma(1-\gamma_5)v_{\bar{\nu}_e} \tag{38}$$

where the factor in brackets corresponds to the W propagator. In muon decay, $|q^2| \ll m_W^2$, hence Eq. (38) reduces to Eq. (37) if we put $G/\sqrt{2} = g^2/8m_W^2$. Thus,

$$m_W^2 = \frac{\pi\alpha}{\sqrt{2}\,G\sin^2\theta}\frac{1}{} = \frac{(37.5\ \text{GeV})^2}{\sin^2\theta} \tag{39}$$

and

$$m_Z^2 = \frac{m_W^2}{\cos^2\theta} = \frac{(27.5\ \text{GeV})^2}{\sin^2\theta} \ . \qquad (40)$$

From Eqs. (35) and (36) we may also obtain an effective current-current lagrangian for neutral weak processes in the limit $q^2 << m_Z^2$. This is:

$$\mathcal{L}_{\text{eff}} = -\sqrt{2}\, G J_N^{\lambda} \cdot J_{N\lambda} \qquad (41)$$

In order to apply Eq. (41) to the neutral weak e-N coupling in low energy atomic physics we must obtain matrix elements of $J_{N\lambda}$ between physical nucleon states in the limit of zero momentum transfer (Weinberg 1972). Application of simple isospin arguments, of the conserved vector current hypothesis, and neglect of all momentum-transfer dependent terms, results in the following amplitudes:

$\mathcal{A}(ep \to ep) =$

$$-\frac{G}{2\sqrt{2}}\, \bar{u}'_e \gamma_\lambda (1 - 4\sin^2\theta - \gamma_5) u_e \cdot \bar{u}'_p \gamma^\lambda (1 - 4\sin^2\theta - g_A\gamma_5) u_p \qquad (42)$$

$$\mathcal{A}(en \to en) = +\frac{G}{2\sqrt{2}}\, \bar{u}'_e \gamma_\lambda (1 - 4\sin^2\theta - \gamma_5) u_e \bar{u}'_n \gamma^\lambda (1 - g_A\gamma_5) u_n \qquad (43)$$

Thus for a nucleus with Z protons and N neutrons, the $A_e V_n$ component is:

$$\mathcal{A}(A_e V_N) = +\frac{G}{2\sqrt{2}}\, [(1 - 4\sin^2\theta)Z - N] \bar{u}'_e \gamma_\lambda \gamma_5 u_e \cdot \bar{\psi}'_N \gamma^\lambda \psi_N \qquad (44)$$

where $\psi_N$ is a nucleon spinor. In the N.R. limit.,

$$\psi_N \to \begin{pmatrix} \chi_N \\ 0 \end{pmatrix}$$

where $\chi_N$ is a two-component Pauli spinor. Thus $\bar{\psi}'_N \gamma^\lambda \psi_N = \chi'^{\dagger}_N \chi_N, (=0)$; if $\lambda = 0$, (=1,2,3); and we obtain Eq. (7). The non-relativistic limit of the electron [Eq. (8)] is easily obtained by noting that

$$\gamma_5 = \begin{pmatrix} 0 & 1 \\ 1 & 0 \end{pmatrix}$$

and

$$u_e \approx \begin{pmatrix} \chi_e \\ \frac{\vec{\sigma}\cdot\vec{p}_e}{2m_e c}\ \chi_e \end{pmatrix}$$

Similar considerations apply to Eq. (9).

# 3. POLARIZED ELECTRON-NUCLEON SCATTERING

## 3.1 Theoretical Analysis

We now consider the helcity-dependent asymmetry in scattering of high energy polarized electrons by nucleons, measured in the experiment at SLAC (Prescott et al 1978, 1979). Our discussion here is initially independent of any particular gauge theory, and follows the treatment of Cahn & Gilman (1978) who employed the quark-parton model. Here the nucleon is assumed to consist of three "valence" quarks plus a "sea" of virtual quark-antiquark pairs. This is appropriate in the regime of large energies and momentum-transfers actually used, where electron and quark-parton masses may be neglected. In this limit $(1 \pm \gamma_5)/2$ are $\pm$ helicity projection operators, respectively, while vector $(\gamma^\mu)$ and axial vector $(\gamma^\mu\gamma_5)$ interactions preserve helicity. The photon couples to quark or electron through the vector current $\gamma_\mu$ with a strength given by its charge $Q_f^\gamma$. Using $\gamma_\mu = \gamma_\mu(1 + \gamma_5)/2 + \gamma_\mu(1 - \gamma_5)/2$ we may define left- and right-handed charges

$$Q_{Lf}^\gamma = Q_{Rf}^\gamma = Q_f^\gamma. \tag{45}$$

The $Z^o$ couples to left- and right-handed fermions with strengths $Q_{Lf}^Z$ and $Q_{Rf}^Z$, respectively; these are in general different. Thus the $Z^o$-fermion Dirac vertex has the form:

$$Q_{Rf}^Z \gamma_\mu \frac{(1 + \gamma_5)}{2} + Q_{Lf}^Z \gamma_\mu \frac{(1 - \gamma_5)}{2} . \tag{46}$$

Now consider the scattering of electron and quark in the CM frame. It is easy to show that if both (massless) fermions have the same helicity, the scattering is isotropic, while if they have opposite helicity, the angular distribution is proportional to $(1 + \cos\hat{\theta})^2$, where $\hat{\theta}$ is the

scattering angle. In both cases the helicity of each fermion remains unchanged in the scattering process. In the lab frame this translates into a dependence of the differential cross-section on $y = 1 - E'/E \equiv \nu/E$ where E' and E are the final and initial lepton energies, respectively. Recalling that the electromagnetic and weak interactions contribute coherently to the amplitude for each quark, we easily obtain the following results for the differential cross-sections:

RH $e^-$ on RH quark of type i:

$$d\sigma \propto \left| \frac{Q^{\gamma}_{Re} Q^{\gamma}_{Ri}}{q^2} + \frac{Q^{Z}_{Re} Q^{Z}_{Ri}}{q^2 - m_Z^2} \right|^2 ; \tag{47}$$

RH $e^-$ on LH quark of type i:

$$d\sigma \propto \left| \frac{Q^{\gamma}_{Re} Q^{\gamma}_{Li}}{q^2} + \frac{Q^{Z}_{Re} Q^{Z}_{Li}}{q^2 - m_Z^2} \right|^2 (1 - y)^2 ; \tag{48}$$

LH $e^-$ on LH quark of type i:

$$d\sigma \propto \left| \frac{Q^{\gamma}_{Le} Q^{\gamma}_{Li}}{q^2} + \frac{Q^{Z}_{Le} Q^{Z}_{Li}}{q^2 - m_Z^2} \right|^2 ; \tag{49}$$

LH $e^-$ on RH quark of type i:

$$d\sigma \propto \left| \frac{Q^{\gamma}_{Le} Q^{\gamma}_{Ri}}{q^2} + \frac{Q^{Z}_{Le} Q^{Z}_{Ri}}{q^2 - m_Z^2} \right|^2 (1 - y)^2 . \tag{50}$$

The asymmetry for longitudinally polarized $e^-$:

$$\Delta = \frac{d\sigma_R - d\sigma_L}{d\sigma_R + d\sigma_L} \tag{51}$$

is now computed simply by multiplying Eqs. (47) - (51) by the probability $f_i(x)$ of finding a quark of type i with fractional longitudinal

momentum $x = -q^2/2m_p\nu$ in the nucleon and noting that the differential cross sections $d\sigma_{R,L} = d\sigma_{R,L}(x,y)$ involve an incoherent sum over LH, RH quarks in the unpolarized nucleon. Recalling that $Q^\gamma_{Le} = Q^\gamma_{Re} = Q^\gamma_e = -e$, and $Q^\gamma_{Li} = Q^\gamma_{Ri}$, and putting $g_V = (Q^Z_R + Q^Z_L)/2$ and $g_A = (Q^Z_R - Q^Z_L)/2$, we obtain, to order $-q^2/m_Z^2$:

$$\Delta(x,y) = -\frac{(-2q^2)}{m_Z^2}\,\frac{\sum_i f_i(x)\,(Q^\gamma_i/e)\left(g_{A,e}g_{V,i} + \frac{[1-(1-y)^2]}{[1+(1-y)^2]}\,g_{V,e}g_{V,i}\right)}{\sum_i f_i(x)\,(Q^\gamma_i)^2} \tag{52}$$

The sum over quark types i in Eq. (52) must include both quarks and antiquarks at a given x. However, for $x \gtrsim 0.2$ it is known from various deep-inelastic scattering experiments that antiquarks may safely be neglected, and we confine ourselves to this region henceforth. Also we now restrict ourselves to SU(2)×U(1) (but not yet to the Weinberg-Salam model). Then the weak charges of the fermions are given by

$$Q^Z_L = \frac{e}{\sin\theta\cos\theta}\,(L_3 - Q^\gamma \sin^2\theta) \tag{53}$$

$$Q^Z_R = \frac{e}{\sin\theta\cos\theta}\,(R_3 - Q^\gamma \sin^2\theta) \tag{54}$$

where $L_3$ and $R_3$ are the third-components of the weak isospin for left, right-handed fermions, respectively, as in Section 2. In the Weinberg-Salam model, of course, $L_3 = +\frac{1}{2}$ for up-quark, $L_e = -\frac{1}{2}$ for down-quark and electron, and $R_3 = 0$ for all fermions. Also for an isosinglet target (deuterium), $f_u(x) = f_d(x)$. Assuming this, neglecting antiquarks, and employing conventional $L_3$ assignments, we obtain from Eq. (52) the formula:

$$\frac{\Delta_{e,d}(x,y)}{(-q^2)} = a_1 + a_2\left[\frac{1-(1-y)^2}{1+(1-y)^2}\right] \tag{55}$$

where

$$a_1 = -\frac{G}{2\sqrt{2\pi}\,\alpha}\frac{9}{10}(1 + 2R_3^e)(1 - \frac{20}{9}\sin^2\theta + \frac{4}{3}R_3^u - \frac{2}{3}R_3^d) \quad (56)$$

and

$$a_2 = -\frac{G}{2\sqrt{2\pi}\,\alpha}\frac{9}{10}(1 - 4\sin^2\theta - 2R_3^e)(1 - \frac{4}{3}R_3^u + \frac{3}{2}R_3^d). \quad (57)$$

The quantity $\Delta_{ed}/(-q^2)$ is plotted in Figure 2 as a function of y for various SU(2)×U(1) models, identified by their assignment of RH fermions. The Weinberg-Salam model has right-handed isosinglets only. The other models place the RH electron in a weak isodoublet with a hypothetical neutral heavy lepton $E_o$ ("hybrid" model) or assume one or more of the quarks to be in RH doublets. In the past, models based on other gauge groups have also been considered. Most of the $SU(2)_L \times SU(2)_R \times U(1)$ models predict no parity violation: $\Delta_{e,d}(x,y) = 0$. Most of the other models [SU(3)×U(1), SU(3)×SU(3), etc.] are ruled out by the results of neutrino experiments.

## 3.2 The SLAC Experiment

The asymmetry Δ was measured in the scattering of 19.4 GeV polarized electrons on a stationary target (Prescott et al 1979). Since Δ is expected to be small, ($\Delta \approx 10^{-4}$), the experimenters abandoned traditional single particle counting techniques. On each 1.5 μs pulse of the accelerator, they detected $\sim 10^3$ scattered electrons in the same detector and integrated the total signal. In this way a statistical precision of $10^{-5}$ was possible after only $10^7$ pulses, or about 1 day's running.

POLARIZED ELECTRON SOURCE A block diagram of the experiment is shown in Figure 3. The polarized electrons were produced in a GaAs

crystal by exciting transitions from the J = 3/2 valence band to the J = ½ conduction band with circularly polarized 7100 Å light from a flashlamp pumped dye laser. These conduction electrons then left the surface of the crystal and were injected into the Linac. The maximum possible polarization obtainable in this way is P = .5, but during the actual experiment, P ≃ .37. P was measured every eight hours by Møller scattering of the electrons on a magnetized iron foil placed behind the target. (The target was removed for the polarization measurement.) A statistical precision of 3% in P was obtained in 20 minutes. The helicity of the beam could be reversed by reversing the polarization of the light. This was accomplished in two ways. The light was first linearly polarized with a Glan-Air prism, and then circularly polarized with a Pockels cell. The sign of the voltage on the Pockels cell was chosen randomly from pulse to pulse: sign reversal changes the polarization of the light. The Glan polarizer could also be rotated by 90°, which reverses the circular polarization as well. In addition, unpolarized electrons could be produced, either by substituting the normal thermionic SLAC source for the GaAs crystal, or by rotating the Glan prism 45°, in which case the Pockels cell has no retardation effect.

Approximately $3 \times 10^{12}$ electrons per pulse were injected into the Linac, and about $10^{11}$ electrons remained after acceleration. The beam energy and position were carefully monitored and stabilized by computer-controlled feedback loops. After acceleration, the beam was bent through an angle of 24.5° in the SLAC switchyard to reach the experimental area. The highly relativistic electrons underwent a precession of

$$\theta = \gamma \frac{(g-2)}{2} = \frac{E\pi}{3.237}$$

where $\gamma = E/m_e$, g-2 is the anomaly in the electron g-factor, and E is in GeV. The beam was longitudinally polarized only when E/3.237 = integer. This provided a source-independent way of reversing the electron helicity or making it zero.

TARGET AND SPECTROMETER After passing through the beam transport system, the electrons struck a 30 cm target containing liquid $D_2$. Electrons which scattered at 4° in the vertical plane entered the spectrometer, which analyzed the momentum in the horizontal plane and accepted a very broad momentum range, as shown in Figure 4. For most of the experiment, the beam energy was 19.4 GeV, and the momentum acceptance peaked at 14.5 GeV/c. Note that electrons from elastic and resonant scattering also fall within the acceptance range. These contributed a few percent to the cross section. Figure 4 also shows the pion cross section. Since individual particles cannot be discriminated against in a flux counting experiment, the kinematics were chosen to reduce the $\pi$, K, and $\mu$ background to a few percent.

DETECTORS Two electron detectors were used: a Cerenkov counter and a lead-glass shower counter. They were placed in series, as shown in Figure 3. Since coincidence counting techniques could not be used, the detectors each measured the asymmetry separately. The Cerenkov counter was filled with $N_2$ at atmospheric pressure. A single spherical mirror focused the light onto a photomultiplier tube. The shower counter consisted of nine radiation lengths of lead glass viewed by four photomultipliers. During the second experimental run the data from the two halves of the counter, each representing half of the momentum acceptance, were analyzed separately, thereby providing an asymmetry

at two values of y simultaneously. The properties of the detectors are summarized in Table 2.

Behind the shower counter was 6" of lead, which absorbed electrons. The background particles ($\pi$,K,$\mu$) penetrated this barrier or formed hadronic showers, and were detected by a shower counter behind it. The background asymmetry was observed with this detector, and found to give less than a 1% correction to the final measurement, and consistent with zero.

DATA Data collection was divided into runs of approximately 3.5 hours each. During each run the Pockels cell polarization reversed randomly from pulse to pulse. In between runs, changes were made which reversed the helicity relative to the Pockels cell voltage or eliminated it altogether. These were (1) rotation of the Glan prism by 45° (null experiment) or 90° (polarization reversal); and (2) changes of the beam energy by an amount causing the electrons to precess in the switchyard by integral (reversal) or half integral (null) multiples of $\pi$. The changes in $\Delta$ under these conditions are shown in Figs 5 and 6.

## 3.3 Results of the SLAC Experiment

Data were obtained with an $e^-$ beam energy of 19.4 GeV, and at values of y corresponding to scattered $e^-$ energies from 10.2 to 16.3 GeV. Corrections for radiative effects were made by assuming that $\Delta_{ed}$ has kinematic dependence given by Eq. (55) and by applying previously measured cross sections and radiative correction formulae (3% correction). Higher order weak processes were ignored. The errors assigned to the data arose mainly from counting statistics with some contribution from uncertainty in beam polarization. However, there were also contributions to the

uncertainty from systematic errors: imbalance in beam parameters ($\sim .025$ $\Delta_{ed}$), and uncertainty in beam polarization P ($\sim 2.5\%$).

Figure 7 displays the corrected experimental asymmetry as a function of y. Even preliminary data at low values of y ruled out $SU(2)_L \times SU(2)_R \times U(1)$ models and $SU(2) \times U(1)$ models other than the Weinberg-Salam and the "hybrid." The best-fit y dependencies of these latter two are displayed in Figure 7 along with a model-independent parametrization of the data assuming only the form of Eq. (55) with $a_1$ and $a_2$ as constants to be determined. The results are clearly consistent with the Weinberg-Salam model, and give a best fit of $\sin^2\theta = 0.224 \pm 0.020$ with a $\chi^2$ probability of 40% (a value in good agreement with that obtained in neutrino experiments). The results are just as clearly inconsistent with the hybrid model; here, a best fit gives $\sin^2 \theta = 0.015$ (widely at variance with neutrino results) and a $\chi^2$ probability of $6 \times 10^{-4}$. The best fit for model-independent parameters is

$$a_1 = -(9.7 \pm 2.6) \times 10^{-5} \tag{58}$$

$$a_2 = (4.9 \pm 8.1) \times 10^{-5}. \tag{59}$$

Further discussion of these results will be given in Section 5.

# 4. PARITY VIOLATION IN ATOMS

## 4.1 Hydrogenic Atoms

ANALYSIS All hydrogenic atom experiments now being pursued utilize the special properties of the $2^2S_{\frac{1}{2}}$ and $2^2P_{\frac{1}{2}}$ states (see Figure 8). At zero magnetic field B, the $2^2S_{\frac{1}{2}}$ and $2^2P_{\frac{1}{2}}$ levels are separated by the Lamb shift S = 1058 MHz. The natural lifetime of $2^2P_{\frac{1}{2}}$ is short [$\tau(2P) = 1.6 \times 10^{-9}$ s] since a 2P atom can decay to the ground state by allowed E1 photon emission (Lyman $\alpha$). The 2P state has natural width $\Gamma_{2p}$ = 100 MHz. In the absence of external electric fields (which mix 2P and 2S by Stark effect) the $2^2S_{\frac{1}{2}}$ state is metastable [$\tau(2S)$ = 1/8 s] since its only effective mode of decay is by two-photon emission. Thus one can form a beam of 2S atoms which exists over the length of a practical apparatus (meters). The zero B field hyperfine structure splittings (hfs) of the $2^2S_{\frac{1}{2}}$ and $2^2P_{\frac{1}{2}}$ states are precisely calculable, as is the Zeeman effect; and the $2^2S_{\frac{1}{2}}$ hfs splitting has been measured accurately. Parity violation causes a mixing of $2^2S_{\frac{1}{2}}$ and $2^2P_{\frac{1}{2}}$ Zeeman components with the same $m_F$ (e.g., the levels $\beta_o e_o$ or $\beta_o f_o$ in ${}_1H^1$.) The matrix elements $\langle e_o|H_p|\beta_o\rangle$, etc. are extremely small, but by way of compensation the effective energy denominator $\Delta E$ in Eq. (11) is also small. It is in fact, $\Delta E = \Delta E_o + i\Gamma_{2p}/2$ where $\Delta E_o$ is the real energy separation ($\Delta E_o$ = S at zero magnetic field and $\Delta E_o \to 0$ at a level crossing.)

One may carry out a general analysis of parity violating effects starting from the forms given in Eqs. (4) and (5) (Dunford et al 1978). We begin with the matrix element of $H_p^{(1)}$ in the non-relativistic point-nucleon limit, between states $|\psi\rangle$ and $|\chi\rangle$:

$$\langle\chi|H_p^{(1)}|\psi\rangle = \frac{G}{\sqrt{2}}(\chi^\dagger\gamma_5\psi)_{r=0} \cdot C_1 \tag{60}$$

where $C_1 = ZC_{1p} + NC_{1n}$. Next we carry out a two-component reduction of $(\chi^\dagger\gamma_5\psi)_{r=0}$. In the special case where $\chi$ and $\psi$ correspond to $n^2P_{\frac{1}{2}}$ and $n^2S_{\frac{1}{2}}$ states, respectively, we find

$$\langle n^2P_{\frac{1}{2}}|H_p^{(1)}|n^2S_{\frac{1}{2}}\rangle = iC_1\frac{3G}{\sqrt{2}\ 8\pi}\frac{\hbar}{m_e c}R'_{nP}(0)R_{nS}(0)\delta_{m'_J m_J}\delta_{m'_I m_I} \tag{61}$$

where the R's are Schroedinger radial wavefunctions, and I and J are nuclear and atomic angular momenta, respectively. Employing explicit values for the R's we obtain:

$$\langle n^2P_{\frac{1}{2}}|H_p^{(1)}|n^2S_{\frac{1}{2}}\rangle = iC_1\bar{V}\delta_{m'_J m_J}\delta_{m'_I m_I} \tag{62}$$

where

$$\bar{V} = \frac{G}{2\pi\sqrt{2}\ a_o^3}\left(\frac{Z}{n}\right)^4 (n^2-1)^{\frac{1}{2}}$$

$$= .118\left(\frac{Z}{n}\right)^4 (n^2-1)^{\frac{1}{2}}\ \text{hz}. \tag{63}$$

Similarly, for $H_p^{(2)}$, one obtains:

$$\langle n^2P_{\frac{1}{2}}|H_p^{(2)}|n^2S_{\frac{1}{2}}\rangle = -2i\bar{V}C_2\langle m'_J m'_I|\vec{\sigma}_e\cdot\vec{I}|m_J m_I\rangle \tag{64}$$

where $C_2 = C_{2p}$ for hydrogen, and $C_2 = \frac{1}{2}(C_{2p} + C_{2n})$ for deuterium (neglecting the small $^3D_1$ component in the nuclear wavefunction). In terms of individual hyperfine components $|Fm_F\rangle$, the matrix elements are

$$\langle n^2P_{\frac{1}{2}},F'm'_F|H_p^{(1)}|n^2S_{\frac{1}{2}},Fm_F\rangle = iC_1\bar{V}\delta_{F'F}\delta_{m'_F m_F} \tag{65}$$

$$\langle n^2P_{\frac{1}{2}},F'm'_F|H_p^{(2)}|n^2S_{\frac{1}{2}},Fm_F\rangle = -2i\bar{V}C_2\delta_{F'F}\delta_{m'_F m_F}[F(F+1) - I(I+1) - (3/4)] \tag{66}$$

We next consider the effect of an external magnetic field B (Zeeman effect). For $2^2S_{\frac{1}{2}}$, $2^2P_{\frac{1}{2}}$ states the energy levels of hydrogen in finite B

are shown in Figure 8. The states $\alpha_{+1}$, $\alpha_o$, $\beta_o$, etc. may be expressed in terms of states $|2L_{\frac{1}{2}},m_J,m_I\rangle$ as follows:

$$
\begin{aligned}
|\alpha_{+1}\rangle &= |2S_{\frac{1}{2}},+\tfrac{1}{2},+\tfrac{1}{2}\rangle \\
|\alpha_o\rangle &= \cos\Theta_S|2S_{\frac{1}{2}},\tfrac{1}{2},-\tfrac{1}{2}\rangle + \sin\Theta_S|2S_{\frac{1}{2}},-\tfrac{1}{2},\tfrac{1}{2}\rangle \\
|\beta_o\rangle &= \cos\Theta_S|2S_{\frac{1}{2}},-\tfrac{1}{2},\tfrac{1}{2}\rangle - \sin\Theta_S|2S_{\frac{1}{2}},\tfrac{1}{2},-\tfrac{1}{2}\rangle \\
|\beta_{-1}\rangle &= |2S_{\frac{1}{2}},-\tfrac{1}{2},\tfrac{1}{2}\rangle \\
|e_{+1}\rangle &= |2P_{\frac{1}{2}},\tfrac{1}{2},\tfrac{1}{2}\rangle \\
|e_o\rangle &= \cos\Theta_P|2P_{\frac{1}{2}},\tfrac{1}{2},-\tfrac{1}{2}\rangle + \sin\Theta_P|2P_{\frac{1}{2}},-\tfrac{1}{2},\tfrac{1}{2}\rangle \\
|f_o\rangle &= \cos\Theta_P|2P_{\frac{1}{2}},-\tfrac{1}{2},\tfrac{1}{2}\rangle - \sin\Theta_P|2P_{\frac{1}{2}},\tfrac{1}{2},-\tfrac{1}{2}\rangle \\
|f_{-1}\rangle &= |2P_{\frac{1}{2}},-\tfrac{1}{2},+\tfrac{1}{2}\rangle
\end{aligned}
\tag{67}
$$

where

$$\cos\Theta_{S,P} = x_{S,P}[x_{S,P}^2 + (\sqrt{x_{S,P}^2 + 1} - 1)^2]^{-\frac{1}{2}},$$

$$x_{S,P} = \frac{[g_{J,(S,P)} + g_I]\mu_o B}{a_{S,P}}$$

and $a_{S,P}$ = zero field hfs splitting. (In fact, $\Theta_S \approx \Theta_P$ and the S,P subscripts may be disregarded.) From formulae (67) it is easy to show that the only non-zero matrix elements of $H_p$ between states crossing in a magnetic field are:

$$\langle e_o|H_p|\beta_o\rangle = -2C_{2p}\cos 2\Theta \cdot i\bar{V} \tag{68}$$

$$\langle f_o|H_p|\beta_o\rangle = [C_{1p} + (1 + 2\sin 2\Theta)C_{2p}]i\bar{V} \tag{69}$$

$$\langle f_{-1}|H_p|\beta_{-1}\rangle = (C_{1p} - C_{2p})i\bar{V}. \tag{70}$$

Note that mixing of $e_o$ and $\beta_o$ involves only $C_{2p}$; thus according to the Weinberg-Salam model the matrix element is proportional to the small

quantity $C_{2p} = .62(1 - 4\sin^2\theta) \sim .05$ for $\sin^2\theta = .23$. Similar formulae to Eqs. (68) - (70) are easily obtained for deuterium and tritium.

We now consider the mixing of $2^2S_{\frac{1}{2}}$ and $2^2P_{\frac{1}{2}}$ components, according to the equation:

$$|2^2S_{\frac{1}{2}}\rangle' = |2^2S_{\frac{1}{2}}\rangle + \frac{\langle 2^2P_{\frac{1}{2}}|H_P|2^2S_{\frac{1}{2}}\rangle}{E_{2^2S_{\frac{1}{2}}} - E_{2^2P_{\frac{1}{2}}}} \cdot |2^2P_{\frac{1}{2}}\rangle. \qquad (71)$$

As noted previously in the energy denominator we must include a term for damping of the 2P state:

$$E_{2S} - E_{2P} = \Delta E_o + i\frac{\Gamma_{2p}}{2} \qquad (72)$$

where $\Gamma_{2p} = 100$ MHz, and $\Delta E_o$ is the real part of the energy splitting. Also, $\Delta E_o$ is variable in a magnetic field B because of Zeeman effect; e.g., it becomes zero at the $\beta_o e_o$ crossing at 545 Gauss; or the $\beta_o f_o$ crossing at 1160 Gauss. For the $\beta_o e_o$ crossing we find from Eqs.(68) and (63),(64):

$$\frac{\langle 2^2P_{\frac{1}{2}}, e_o|H_P|2^2S_{\frac{1}{2}}, \beta_o\rangle}{i\Gamma_{2p}/2} = -2C_2\,\frac{(.013\text{ Hz})}{100\text{ MHz}} = -2.6\times 10^{-10}\,C_2. \qquad (73)$$

SCALARS AND PSEUDOSCALARS From Eq. (73) it is plain that parity violating effects in hydrogenic atoms are exceedingly small. In order to design effective experiments to detect them it is useful to consider all possible scalar and pseudoscalar forms which can be constructed from the various vectors describing experimental arrangements. (Such an exercise is also helpful for heavy atom experiments.) In general, the relevant vectors are external static electric ($\vec{E}$) and magnetic ($\vec{B}$) fields, electric vector $\hat{\epsilon}$ and direction $\hat{k}$ of a light beam, $\hat{\epsilon}_R$, $\hat{k}_R$ and magnetic vector $\hat{m}_R$ for a microwave field ($\hat{\epsilon}_R$ and $\hat{m}_R$ are not necessarily

orthogonal), initial and final atomic polarization $\vec{J}$, and so on. Any term, scalar or pseudoscalar, appearing in the transition probability W, must be expressible in terms of these vectors. However, whether a term actually appears in W, and if so, its magnitude, depends on detailed physical arguments rather than the present symmetry considerations.

For example consider a circular dichroism experiment. Here the only available vectors are those describing a circularly polarized light beam, namely $\hat{k}$ and $\hat{\varepsilon}$ (which is complex). The only pseudoscalar we can form is $i\hat{\varepsilon}^* \times \hat{\varepsilon} \cdot \hat{k}$, which is the photon helicity h.

Certain general considerations restrict our choice of possible forms. First, since reversal of $\hat{\varepsilon}$ produces no physical change, any acceptable term must contain only even powers of $\hat{\varepsilon}$ (as in $h = i\hat{\varepsilon}^* \times \hat{\varepsilon} \cdot \hat{k}$). Next, if $\vec{E}$ appears in a pseudoscalar term, it is contained in a Stark amplitude which interferes with $\mathcal{E}_p$; thus $\vec{E}$ must appear linearly. Third, under time reversal (T), $\vec{E} \to \vec{E}$, $\vec{B} \to -\vec{B}$, $\hat{\kappa} \to -\hat{k}$, $\hat{\varepsilon} \to \hat{\varepsilon}$, $\hat{m} \to -\hat{m}$, $h \to h$, and $\vec{J} \to -\vec{J}$. If damping is negligible (the case for all heavy atom experiments and hypothetical hydrogenic atom experiments in which 2S - 2P level separations are large compared to $\Gamma_{2p}$), then scalar and pseudoscalar terms must be even under T. (We assume T-invariance.) for example, $(\hat{\varepsilon} \cdot \vec{B})(\hat{\varepsilon} \cdot \vec{E}\times\vec{B})$ is a T-even pseudoscalar and an acceptable possibility, while $(\hat{\varepsilon} \cdot \hat{\varepsilon})(\vec{E} \cdot \vec{B})$ is T-odd and thus unacceptable. However, if damping is important (as in hydrogen experiments where 2S - 2P level separations are small compared to $\Gamma_{2p}$) then it can be shown that formally T-odd terms are acceptable (Bell 1979). Loosely speaking, this occurs because an extra factor of i

appears in $\mathcal{E}_p$, due to $\Delta E = \Delta E_o + (i\Gamma/2) \rightarrow i\Gamma/2$. An example of a pseudoscalar term which is acceptable in these circumstances, though formally T-odd, is $(\hat{\epsilon}_R \cdot \vec{E})(\hat{\epsilon}_R \cdot \vec{B})$. Dunford et al (1978) have given a complete list of possible scalar and pseudoscalar terms for hydrogen experiments.

EXPERIMENTS Experiments are now underway at Seattle (Trainor 1979), Michigan (Dunford et al 1978), and Yale (Hinds 1979). The important parameters in each experiment are summarized in Table 3. Each employs a beam of $2^2S_{\frac{1}{2}}$ atoms traveling along a coaxial B field. The beam is polarized, and then enters one or more resonance regions where transitions are induced to another $2^2S_{\frac{1}{2}}$ state at a 2S - 2P level crossing. At present, each experiment is designed to work at the $\beta_o e_o$ crossing and is thus sensitive to $C_{2p}$. Future extensions to the $\beta_o f_o$ and $\beta_{-1} f_{-1}$ crossings and the use of deuterium or tritium as well as hydrogen may permit measurements of all four coupling constants.

Since the parity mixing indicated by Eq. (73) is so small, efforts must be made to suppress the parity conserving amplitude as much as possible, but this results in low counting rates and dilution of signal by background. Asymmetries at the $10^{-7}$ level are expected if the coupling constants are described by the Weinberg-Salam model.

In the Michigan experiment (Figure 9) a metastable beam is produced by passing a proton beam from a duoplasmatron source through a cesium charge transfer canal, which yields a flux of $\sim 10^{14}$ atoms/s in the 2S state. A 575 Gauss magnetic field is applied in the "β quench" region, and an electric field mixes β and e states, causing decay of all β's. The beam, now pure α, continues to the interaction region, which consists of a $TM_{0,0}$ cylindrical microwave cavity which is tilted

at an angle $\phi = 5°$ with respect to the beam axis and $\vec{B}$, and tuned to the $\alpha_o\beta_o$ transition. The rf polarization $\hat{\epsilon}_R$ is along the cavity axis. A dc electric field $\vec{E}$ of 1 V/cm Stark-mixes $\beta_o$ and $e_-$ states. $\vec{E}$ is applied perpendicular to $\vec{B}$, with thin wire electrodes inside the cavity. The $\alpha_o\beta_o$ transition rate is proportional to

$$r_s(\hat{\epsilon}_R\times\vec{B})^2(\vec{E}\times\vec{B})^2 + r_p(\hat{\epsilon}_R\cdot\vec{E})(\hat{\epsilon}_R\cdot\vec{B}) \qquad (74)$$

where the term in $r_s(r_p)$ is scalar (pseudoscalar). (As we have noted, the pseudoscalar term is formally T-odd.) It is clear from expression (74) that the transition rate exhibits an asymmetry with respect to reversal of $\vec{E}$ or $\vec{B}$, or if $\phi \to -\phi$. The asymmetry is detected by selective quenching of $\beta_o$ atoms in the detection region downstream.

With present running conditions of $10^{13}$ $\alpha_o$ atoms per second and an $\alpha_o \to \beta_o$ conversion fraction of $5 \times 10^{-6}$, the expected detection rate is $R = 10^7(1 \pm 5 \times 10^{-6}\ C_{2p})$ counts/s which should yield a statistical precision equal to the asymmetry in 400 hours for $\sin^2\theta = .23$. At present, the $\alpha_o \to \beta_o$ transition has been observed, but much work remains, and the apparatus just described may be altered considerably before the experiment is completed. Currently, efforts are being made to reduce diluting backgrounds, which may come from such diverse sources as background gas or wall collisions, scattered Lyman-α radiation from the source, or cascades from higher n states. Future work at Michigan will concentrate on detecting and eliminating systematic errors, which have been analyzed by Dunford et al (1978). Reduction of false asymmetries to a level below the signal (for $C_{2p} \simeq .1$) requires beam alignments of better than $10^{-3}$ radians, and electric and magnetic field reversals accurate to $10^{-4}$ or better. Stray electric fields, and the average motional

electric field due to misalignments or divergence of the beam, must be smaller than $5 \times 10^{-6}$ V/cm!

The Seattle experiment is similar, although details of the interaction region differ slightly. The Seattle group employs an rf cavity with $\hat{\varepsilon}_R$ parallel to the beam and $\vec{B}$, and alters the axis of quantization by the small angle $\phi$, by applying a small perpendicular $\vec{B}$ field. A static electric field is applied to cancel out the resultant motional field, in addition to the Stark-mixing $\vec{E}$ field. The $\alpha_o \rightarrow \beta_o$ transition is the same, as are many of the systematic problems, and the experimental parameters and estimated running time are similar. Reduction of stray and motional electric fields may be the chief difficulty in these two experiments. The problem may be simplified by a "separated oscillating fields technique," suggested by E. Hinds of Yale (Hinds 1979) who proposes measuring $C_{2p}$ by driving the transition $\beta_{-1} \rightarrow \beta_o$ near the $\beta_o e_o$ crossing. Unlike the transition $\alpha_o \rightarrow \beta_o$, this is a proton spin-flip. The experiment is done in two separate regions 1 and 2, which contain oscillating fields $\vec{\mathcal{E}}_{R1}$ and $\vec{\mathcal{E}}_{R2}$ (see Figure 10). Region 1 also contains a static field $\vec{E}_1$, and the principal contribution to the $\beta_- \rightarrow \beta_o$ rate is a Stark-induced electric dipole transition in region 1. Region 2 contains no static electric fields, and $\vec{\mathcal{E}}_{R2}$ drives the principal contribution to the PNC electric dipole transition. As long as phase coherence between $\vec{\mathcal{E}}_{R1}$ and $\vec{\mathcal{E}}_{R2}$ is maintained, the total transition rate contains an interference term between these two amplitudes, proportional to the pseudoscalars

$$C_{2p}(\vec{E}_1 \cdot \vec{B})(\vec{\mathcal{E}}_{R1} \times \vec{B})\ (\vec{\mathcal{E}}_{R2} \times \vec{B}) \qquad (75)$$

or

$$C_{2p}(\vec{E}_1 \cdot \vec{B})(\vec{\mathcal{E}}_{R1} \times \vec{\mathcal{E}}_{R2} \cdot \vec{B}), \tag{76}$$

depending on the relative angle of $\vec{\mathcal{E}}_{R1}$ and $\vec{\mathcal{E}}_{R2}$. The scheme has considerable flexibility since the size of the asymmetry now depends not only on $|\vec{E}|$, but also on $|\vec{\mathcal{E}}_{R2}|/|\vec{\mathcal{E}}_{R1}|$, and this together with the fact that the PNC transition takes place in a field-free region may decrease the effects of stray electric fields. The major advantage, however, comes from the ability to change the relative phase of the parity-conserving and non-conserving amplitudes by varying the $\vec{\mathcal{E}}_{R1}$, $\vec{\mathcal{E}}_{R2}$ phase. During the experiment this will be rapidly varied back and forth by $\pi$, which reverses the sign of the interference term. In addition, sign changes occur for $\vec{E}_1 \rightarrow -\vec{E}_1$ and $\vec{B} \rightarrow -\vec{B}$. The observed asymmetry can also be distinguished by its magnetic field-dependence near the $\beta_o e_o$ crossing, which differs from the field dependence of stray or motional field asymmetries.

Hinds has carried out an extensive study of possible systematic errors, and has concluded that stray E fields must be kept to the level of $\sim 3 \times 10^{-4}$ V/cm in region 2, and average beam alignment to $10^{-4}$ radians. The pseudoscalar contribution to the overall rate is expected to be $1.5 \times 10^{-5}\ C_{2p}$, and a precision of 1 $\sigma$ after 16 hours of running is expected. Since the $\beta_{-1} \rightarrow \beta_o$ transition is a nuclear spin flip, it is relatively insensitive to backgrounds caused by collisions or stray light. The resonance region can be longer than in the Michigan and Washington experiments because of the lower frequency (100 MHz vs. 1.5 GHz) and this results in greater sensitivity.

The advantages of the two-cavity experiment are not restricted to nuclear spin transitions, but may be equally well applied to the

$\alpha_o$-$\beta_o$ experiments. Such modifications are currently under investigation at Washington and Michigan.

In one version, under study at Washington, the Stark-effect transition occurs in the first cavity, in which $\vec{E}_1$ and $\vec{\mathcal{E}}_{R1}$ are both perpendicular to the beam. The second cavity has $\vec{\mathcal{E}}_{R2}$ along the beam. The $\vec{\mathcal{E}}_{R1}$, $\vec{\mathcal{E}}_{R2}$ phase is adjusted for maximum weak-EM interference. This scheme has the added advantage that the large Stark-allowed $\alpha_+\beta_o$ and $\alpha_o\beta_-$ transitions, which cause backgrounds in the one-cavity experiment, cannot occur with $\vec{\mathcal{E}}_{R1} \parallel \vec{E}_1$.

In addition to the atomic hydrogen experiments described so far, experiments involving the decay of muonic hydrogenic atoms have also been suggested (Moskalev 1974a,b).

4.2 Heavy Atoms

GENERAL CONSIDERATIONS Two parity violating effects turn out to be of practical importance for heavy atoms. These are "optical rotation," and "circular dichroism," each of which may be understood from consideration of the "M1" transition

$$\gamma + |\psi_1\rangle \rightarrow |\psi_2\rangle$$

using circularly polarized photons. If $\hat{k}$ is the direction of photon momentum and $\hat{\epsilon}_\pm = (\hat{i} \pm i\hat{j})/\sqrt{2}$ describes a circular polarization state of helicity $\pm 1$, then $O_{EM}$ in Eq. (11) is:

$$O_{EM} = -\hat{\epsilon}_\pm \cdot \vec{d} - \hat{k}\times\hat{\epsilon}_\pm \cdot \vec{\mu}$$

where $\vec{d}$ and $\vec{\mu}$ are E1 and M1 transition operators, respectively for the atom. From this expression we easily obtain $O_{EM} = -\hat{\epsilon}_\pm \cdot (\vec{d} \mp i\vec{\mu})$, which implies a transition probability

$$W \propto |\mathcal{M}|^2 + |\mathcal{E}_p|^2 \pm 2\mathrm{Im}(\mathcal{E}_p \mathcal{M}^*) \qquad (77)$$

and a characteristic asymmetry $A \sim 2\mathrm{Im}(\mathcal{E}_p)/\mathcal{M}$. From Eq. (11), $\mathcal{E}_p \approx (ea_o/\Delta E)\langle\chi|H_W^{(1)}|\psi_1\rangle$, where a single state $|\chi\rangle$ is assumed to dominate in the sum, and the electric dipole matrix element $\langle\psi_2|O_{EM}|\chi\rangle$ is assumed to be that of an allowed E1 transition, $\sim 3\ ea_o$, where $a_o$ is the Bohr radius. Also, we take $\Delta E$ to be a typical spacing between atomic energy levels $\Delta E \approx .05e^2/a_o$. Now, matrix elements of $H_p^{(1)}$ are non-zero only for atomic orbitals of opposite parity with non-vanishing value/gradient at the origin ($s_{\frac{1}{2}}, p_{\frac{1}{2}}$ orbitals). From Eqs. (7) or (8), one finds: $\langle\chi|H_W^{(1)}|\psi\rangle \approx 10^{-19}(e^2/a_o)Z^3K$ where K is a relativistic correction factor ($K \sim 10$ for $Z \sim 80$). (This was first demonstrated by Bouchiat & Bouchiat 1974b). Thus one obtains:

$$|\mathcal{E}_p| \sim 5 \times 10^{-18}\ ea_o Z^3 K.$$

This is, of course, an extremely small electric dipole amplitude in comparison to allowed E1 transition amplitudes (of order $ea_o$). However, the enhancement factor $Z^3K$ helps considerably for large Z. We find:

$$|\mathcal{E}_p| \approx 10^{-10}\ ea_o \quad \text{for } Z \sim 80. \qquad (78)$$

It is therefore clear why heavy atoms are chosen for study.

In optical rotation experiments, originally suggested by a number of authors (Zeldovich 1959, Khriplovich 1974, Sandars 1975, Soreide & Fortson 1975), a beam of linearly polarized light with frequency close to resonance traverses a cell of length L cm containing an atomic vapor of density N $cm^{-3}$. Optical rotation of the plane of polarization occurs because the linear polarization is a superposition of circular

polarization states (±) which propagate with different indices of refraction $n_\pm$:

$$n_\pm = 1 - \frac{2\pi N_o}{\hbar}\left[\overline{|\mathcal{M}|^2} \pm 2\mathrm{Im}(\mathcal{E}_p \mathcal{M}^*)\right]\left\langle \frac{1}{\omega - \omega_o + (v/c)\omega_o + i(\Gamma/2)}\right\rangle \qquad (79)$$

Here $\omega$ is the photon frequency, $\omega_o$ is the transition frequency, $\Gamma$ is the natural width of the excited state, v is the thermal atomic velocity in the direction of the light beam, and $\langle \ldots \rangle$ indicates an average over the Doppler width of the line. Also the bar over the matrix element squared indicates a sum over final, and average of initial, atomic polarizations. Absorption occurs (by slightly differing amounts for the ± components), with the result that the light emerging from the cell is elliptically polarized. The absorption coefficients are

$$\alpha_\pm = \frac{2\omega}{c}\,\mathrm{Im}(n_\pm). \qquad (80)$$

The optical rotation angle is easily found to be:

$$\phi = \frac{\omega}{2c}\,\ell \cdot \mathrm{Re}(n_+ - n_-) \qquad (81)$$

where $\ell$ is one absorption length. The rotation angle $\phi$ follows a dispersion-like dependence on $\omega - \omega_o$, and near resonance,

$$\phi_{max} \approx \ell\,\frac{\mathrm{Im}(\mathcal{E}_p)}{\mathcal{M}}\,.$$

For experiments actually performed on the allowed M1 transitions in bismuth, Z = 83 (see Figure 11):

$6p^3$, J = 3/2 (ground state) → $6p^3$, J = 5/2 $\quad \lambda$ = 648 nm

$6p^3$, J = 3/2 (ground state) → $6p^3$, J = 3/2 $\quad \lambda$ = 876 nm.

$\mathcal{M}$ is approximately one Bohr magneton: $\mathcal{M} \sim ea_o\alpha$. Thus from Eqs. (78) and (82) we estimate

$$\phi_{max}/\ell \sim 10^{-8} - 10^{-7} \text{ radians/abs. length.} \qquad (82)$$

As we shall see, rotations of this order are in fact observed (Barkov & Zolotorev 1978a,b; 1979).

One may also investigate circular dichroism $\delta$ in certain forbidden M1 transitions in heavy atoms (Cs, $6^2S_{\frac{1}{2}} \to 7^2S_{\frac{1}{2}}$), (Tℓ, $6^2P_{\frac{1}{2}} \to 7^2P_{\frac{1}{2}}$) (see Figures 12 and 13). By definition, $\delta = (\sigma_+ - \sigma_-)/(\sigma_+ + \sigma_-)$ where $\sigma_\pm$ are the cross-sections for resonant absorption of circularly polarized photons with helicities ±1. From Eq. (77) we obtain:

$$\delta = \frac{\sigma_+ - \sigma_-}{\sigma_+ + \sigma_-} = \frac{2\mathrm{Im}(\mathscr{E}_p \mathscr{M}^*)}{|\mathscr{M}^2| + |\mathscr{E}_p|^2} \approx \frac{2\mathrm{Im}(\mathscr{E}_p)}{\mathscr{M}} . \qquad (83)$$

The M1 amplitudes in these cases are extremely small: $\mathscr{M} \approx (10^{-4} - 10^{5})$ $ea_o$, and so $\delta = 2\mathrm{Im}(\mathscr{E}_p)/\mathscr{M} \approx 10^{-3} - 10^{-4}$. Unfortunately, full advantage cannot be taken of this relatively large asymmetry because the M1 intensity itself is very small compared to background signals in actual experiments. To overcome this it is necessary to apply an external electric field E which causes Stark mixing of $|\psi\rangle$ with the $|\chi_n\rangle$ and introduces an E1 transition amplitude $\mathscr{E}_S$.

$$\mathscr{E}_S = -e\vec{E} \cdot \left[ \sum_n \frac{\langle \psi_2^o | O_{EM} | \chi_n^o \rangle \langle \chi_n^o | \vec{r} | \psi_1^o \rangle}{E(\psi_1^o) - E(\chi_n^o)} + \frac{\langle \psi_2^o | \vec{r} | \chi_n^o \rangle \langle \chi_n^o | O_{EM} | \psi_1^o \rangle}{E(\psi_2^o) - E(\chi_n^o)} \right] \qquad (84)$$

For sufficiently large E, we obtain: $|\mathscr{E}_S|^2 >> |\mathscr{M}|^2$ and the transition strength becomes greater than background. To detect $\mathscr{E}_p$ one exploits a pseudoscalar interference term $\sim \mathscr{E}_p\mathscr{E}_S$.

CALCULATIONS OF OPTICAL ROTATION For a heavy atom with many (N) electrons calculation of $\mathscr{E}_p$ from Eq. (11) is a formidable problem in atomic theory, containing a number of subtle difficulties. First,

evaluation of matrix elements of $H_P^{(1)}$ requires knowledge of wavefunctions and gradients at the nucleus, where relativistic effects are important. Second, Eq. (11) includes a sum over intermediate states, possibly with significant contributions from the continuum and from states of the form N+1 electrons, 1 positron ($e^+e^-$ "pair" states). Moreover, $\mathscr{E}_P$ may be seriously affected by shielding corrections, especially in the bismuth optical rotation transitions (Harris et al 1978).

Hiller et al (1979) have discussed a basic theoretical framework which makes possible a consistent treatment due to $e^+e^-$ pairs, from which they have shown there is an appreciable contribution. They have also shown that when the Dirac "velocity" operator $\alpha$ is eliminated in favor of the "length" operator $i\omega r$ in the factors $\langle\psi|O_{EM}|\chi\rangle$ appearing in Eq. (11), cancellations occur which result in an accurate formula for $\mathscr{E}_P$, involving only the positive energy N-electron eigenstates of the so-called <u>no-pair</u> Hamiltonian $H_+$. The latter is defined as:

$$H_+ = \sum_{i=1}^{N} H_D(r_i) + L_+\left(\sum_{i<j}^{N} \frac{e^2}{r_{ij}}\right)L_+. \qquad (85)$$

Here $L_+ = L_+(1)....L_+(N)$, where $L_+(i)$ is a positive energy projection operator for the i'th electron, defined by:

$$L_+(i)\phi(r_i) = \Sigma\, u_n(r_i)\, u_n|\phi\rangle,$$

and the u's are normalized <u>positive</u> energy eigenfunctions of the external field one-body Dirac Hamiltonian:

$$H_D = \vec{\alpha}\cdot\vec{p} + \beta m - eA^0_{nuc}(x).$$

Thus specific calculations including only positive energy intermediate states and the length form of the dipole operator are justified. Furthermore, Hiller et al have shown that when the central-field-approximation is used, the sum in Eq. (11) can be extended over negative energy states with very small error, since these states make only minor contributions. This is important for central field calculations utilizing a Green's function approach, in which the sum is automatically carried over all intermediate states.

Bismuth has three equivalent p electrons outside of closed shells, and jj coupling is dominant, though not perfect. Thus Bi has a complex structure, and it is not surprising that calculations of $\zeta_p$ are difficult, and that various estimates in the literature disagree by as much as a factor of 2. In the calculation of optical rotation in bismuth by the Novosibirsk group (Novikov et al 1976, Khriplovich 1979) the closest levels of opposite parity to $6p^3$, namely the $6p^2 7s$ levels are considered, and it is assumed that the 7s electron is added to the $6p^2$ configuration of the Bi II ion without changing the state of the latter. Effective principle quantum numbers of the 6p and 7s electrons are computed from the known energy levels, and the admixture of $6p^2 7s$ states to $6p^3$ states is thus obtained. Numerical calculations of dipole radial integrals are checked by comparing with lifetimes of Bi I excited states. Appreciable contributions also arise from states where a 6s electron is promoted to a 6p orbital: $6s6p^4$. However, the experimental data from Bi II are insufficient to yield numerical values here, so an extrapolation is made from the effective principal quantum number of the 6s electron in Pb and an overall correction factor is applied, since

calculated and observed E1 rates in Pb do not agree. Configuration interaction corrections are found to be relatively small from comparison of calculated and observed hfs splittings. The results are in good agreement with other single-particle calculations using the length form of the dipole operator (see Table 4). However, when one goes beyond this approximation, and employs ab initio methods (e.g., the Hartree-Fock method) the situation becomes complicated and somewhat unsatisfactory. Sandars (1979) has reviewed the various calculations (see Table 4) and has suggested three possible sources of difficulty:

(a) Complications due to the breakdown of jj coupling.

(b) Exchange effects, of special importance when the velocity form of the dipole operator is employed. Possibly there exist large corrections due to pair states in this case, as suggested by Hiller et al (1979).

(c) Shielding effects by parity conserving E1 excitations of the remaining electrons. It has been shown that the importance of this effect diminishes as photon frequency increases, and it is expected to enter but play a relatively minor role in the Cs ($6^2S_{\frac{1}{2}} \rightarrow 7^2S_{\frac{1}{2}}$) and Tl ($6^2P_{\frac{1}{2}} \rightarrow 7^2P_{\frac{1}{2}}$) circular dichroism experiments.

Evidently, more work remains to be done on ab initio calculations of $\mathcal{E}_p$ in bismuth. Finally, we note that in optical rotation experiments one requires knowledge of $\mathcal{M}$ as well as $\mathcal{E}_p$. Although the M1 amplitudes have not been measured directly, they can be calculated quite accurately (see Novikov 1976).

OPTICAL ROTATION EXPERIMENTS Three groups have published results of bismuth optical rotation experiments: Seattle (Lewis et al 1977),

Oxford (Baird et al 1977), and Novosibirsk (Barkov & Zolotorev 1978a,b; 1979). The first two groups independently reported no parity volations at a level which seemed to exclude predictions based on the Weinberg-Salam model; but this was contradicted by the Novosibirsk results, which are in agreement with the predictions of Novikov et al (1976), based on the Weinberg-Salam model. More recently, the Seattle and Oxford groups have also observed parity violation in agreement with predictions of the Weinberg-Salam model.

As noted earlier, the optical rotation per unit absorption length $\phi/\ell$ follows a dispersion shape, and the peaks of dispersion correspond to rotations of $1 - 2 \times 10^{-7}$ radians (see Figure 14). An effect this small cannot be measured with a bismuth cell between crossed polarizers. because the intensity of transmission is proportional to the angle squared. Seattle and Oxford overcome this difficulty by introducing an external optical rotation $\phi_F$ by means of a Faraday cell. This interferes with the optical rotation $\phi_{PNC}$ due to parity violation in a known way. The total intensity of light transmitted through the system is

$$I = I_o[(\phi_{PNC} + \phi_F + \phi_R)^2 + b]$$

where $I_o$ is the incident laser intensity, b is the residual angle-independent transmission through the polarizer (for instance, due to a small birefringence in a window) and $\phi_R$ is any residual optical rotation not caused by parity nonconservation. By varying the magnetic field in the Faraday cell, one modulates $\phi_F$ at frequency $\omega$, and lock-in techniques are employed to isolate the $\omega$-dependent part of the intensity:

$$I_\omega = 2I_o\phi_F(\phi_{PNC} + \phi_R).$$

The signal-to-background ratio is:

$$\frac{I_\omega}{I} \approx \frac{2\phi_F(\phi_{PNC} + \phi_R)}{\phi_F^2 + b} \simeq \frac{(\phi_{PNC} + \phi_R)}{\phi_F^2} \approx 10^{-4} \quad \text{(for Oxford)}$$

where the optimum condition $\phi_F \approx b$ has been assumed. All three groups depend solely on the dispersion shape of $\phi_{PNC}$ to eliminate all possible sources of $\phi_R$, which cannot be distinguished from $\phi_{PNC}$ in any other way.

The Oxford group is working on the 648 nm $^4S_{3/2} \rightarrow {}^2D_{5/2}$ line. This was chosen because at the time it was most accessible to narrow bandwidth CW dye lasers, which must be used to resolve the details of the lineshape. Unfortunately, molecular bismuth absorption in this band limits the density to that corresponding to about one atomic absorption length. Seattle chose the 876 nm $^4S_{3/2} \rightarrow {}^2D_{3/2}$ line which has no molecular absorption, and this permits much higher densities. Recent advances in tunable diode lasers make available a narrow bandwidth source for 876 nm as well.

In both experiments, the light enters the first polarizer and goes through a Faraday cell. Then it enters the bismuth cell, which is enclosed by an oven and surrounded by magnetic shielding. (Magnetic fields must be kept below $10^{-4}$ G because of the Faraday effect in bismuth, which is a serious potential source of $\phi_R$.) The light then passes out of the cell, through the second polarizer, and is detected. The cell contains a buffer gas which keeps the bismuth vapor from condensing on the cool windows. Data are taken by scanning over the hyperfine structure (Seattle) or switching between points of maximum dispersion (Oxford). The Oxford group can move its cell in and out of the beam (see Figure 15a) to perform null experiments.

Other control experiments include the use of a quadrupole resonance or a molecular absorption line, where there is no parity effect.

The Novosibirsk group also employs the 648 nm transition, but instead of modulating a Faraday cell, they deliberately misalign their polarizers by $\theta = \pm 4$ mrad (see Figure 15b). The light which is detected has the form $I = I_o \sin^2(\theta + \phi_{PNC} + \phi_R) \approx \theta^2 I_o[1 + 2(\phi_{PNC} + \phi_R)/\theta]$. A Spectra Physics 375 CW dye laser, operating single mode, is modulated back and forth by 416 MHz every millisecond. The signal is phase-locked to this frequency, and it is proportional to $d\phi_{PNC}/d\lambda$ (see Figure 14). For technical reasons it is only possible to obtain data with the laser frequency centered on the absorption peaks, but null experiments are still possible by locking to quadrupole or molecular lines in the 648 nm band. The angle $\theta$ is reversed every minute or so, and the optics are aligned so that this change does not deviate the beam. The calibration was made by applying a known magnetic field and measuring the Faraday effect. The result of the Novosibirsk experiment may be expressed in terms of $R = \mathrm{Im}(\mathcal{E}_p)/\mathcal{M}$:

$$R_{expt} = (-20.6 \pm 3.2) \times 10^{-8}.$$

This result is in agreement with theoretical calculations of Novikov et al (1976):

$$R_{expt}/R_{theo} = 1.07 \pm 0.14.$$

It yields the value:

$$Q_W(Bi) = -140 \pm 40.$$

CESIUM AND THALLIUM CALCULATIONS For the transitions Cs ($6^2S_{\frac{1}{2}} \rightarrow 7^2S_{\frac{1}{2}}$, $8^2S_{\frac{1}{2}}$) and Tℓ ($6^2P_{\frac{1}{2}} \rightarrow 7^2P_{\frac{1}{2}}$, $7^2P_{3/2}$) relatively straightforward semi-empirical calculations of $\mathcal{E}_p$ are expected to be

reasonably accurate, since the ground state and low-lying excited states of these atoms are quite well described by a single valence electron outside a spherically symmetric core (one-electron central field approximation). Core excitation effects on $\&_p$ are believed to be small in each case and susceptible to effective treatment by perturbation theory.

The first central field calculation was performed by Bouchiat & Bouchiat (1975) who evaluated $\&_p$ for Cs ($6^2S_{\frac{1}{2}} \rightarrow 7^2S_{\frac{1}{2}}$) with a finite sum over $^2P_{\frac{1}{2}}$ terms in Eq. (11). Matrix elements of $H_W^{(1)}$ were calculated by means of a modified Fermi-Segre technique, and relativistic corrections were applied. A correction for the contribution of continuum states was also taken into account. Sushkov et al (1976) employed a somewhat similar semi-empirical method in calculations of $\&_p$(Tℓ, $6^2P_{\frac{1}{2}} \rightarrow 7^2P_{\frac{1}{2}}$), as did Novikov et al (1976) in calculations $\&_p$ (Tℓ, $6^2P_{\frac{1}{2}} \rightarrow 6^2P_{3/2}$). Neuffer & Commins (1977a) also used the central field approximation for $\&_p$ (Tℓ, $6^2P_{\frac{1}{2}} \rightarrow 7^2P_{\frac{1}{2}}$, $6^2P_{3/2}$, $7^2P_{3/2}$) by fitting a modified Tietz potential (which yields a good approximate solution to the Thomas-Fermi equation) to the $6^2P_{\frac{1}{2}}$, $7^2P_{\frac{1}{2}}$ levels of Tℓ and solving the Dirac equation numerically for the valence electron. $\&_p$ was calculated by a finite sum over nearest $^2S_{\frac{1}{2}}$ states and also by means of a Green's function (sum over all states, including auto-ionizing states in the continuum). A similar calculation was carried out on Cs (Neuffer & Commins 1977b). The wavefunctions generated in these calculations were used to compute many auxiliary quantities, which could be compared with atomic-beam and spectroscopic data, especially complete for Cs and Tℓ. These are:

(a) Allowed E1 transition rates and excited state lifetimes (test of wave functions at large r)

(b) Energies and fine structure splittings

(c) Hyperfine structure splittings (test of wavefunctions near the origin, which is especially important for $\mathcal{E}_p$)

(d) Stark-induced E1 amplitudes $\mathcal{E}_S$ [see Eq. (84)]

(e) M1 transition amplitudes

(f) Anomaly in $g_J$ for ground state.

In general, agreement between calculation and experiment for these auxiliary quantities is very satisfactory, when certain configuration-interaction corrections are taken into account; these are of special importance in $(6^2S_{\frac{1}{2}} \rightarrow 7^2S_{\frac{1}{2}})$ and $g_J$ $(6^2S_{\frac{1}{2}})$ for Cs [see Khriplovich (1975), Flambaum et al (1978)]. Thus one has confidence that these one-electron central-field approximation calculations are quite adequate for estimating $\mathcal{E}_p$ to $\approx$ 20% accuracy in each transition. The predicted values of $\mathcal{E}_p$ and $\delta$ for Cs and Tℓ transitions are summarized in Table 5.

CIRCULAR DICHROISM EXPERIMENTS IN CESIUM AND THALLIUM The transition Cs $(6^2S_{\frac{1}{2}} \rightarrow 7^2S_{\frac{1}{2}})$ is being investigated at Paris (Bouchiat & Pottier 1976b, 1979) while parity violation has been observed at Berkeley (Conti et al 1979) in Tℓ $(6^2P_{\frac{1}{2}} \rightarrow 7^2P_{\frac{1}{2}})$, and work continues to refine the result. One of the original motivations for these experiments is that large circular dichroisms $\delta$ are expected according to the Weinberg-Salam model (see Table 5). However, for $\delta$ to be observed directly it would be necessary to detect the M1 transition itself with a signal clearly discernible above background. Unfortunately, this has not been possible so far, because in an actual experiment, one must utilize atomic

vapor at rather high densities in order to achieve acceptable signals. In this case, random local electric fields due to collisions, (and also possibly molecular effects), make it possible for weak photon absorption to occur over a rather broad band of frequencies, and with a strength much larger than that expected from the extremely feeble M1 amplitude. Thus, $\mathcal{M}$ as well as $\mathcal{E}_p$ must be measured indirectly by interference with a Stark-induced E1 amplitude due to external electric field E [Eq. (84)]. It is helpful in considering these effects to proceed with a general analysis of possible scalar and pseudoscalar terms in the transition probability, as was considered for hydrogenic atoms. If we restrict ourselves to <u>linearly</u> polarized light and external E field, and also measure the polarization J of the final atomic state ($7^2S_{\frac{1}{2}}$ in Cs, $7^2P_{\frac{1}{2}}$ in Tℓ), only the following T-invariant scalars representing Stark-M1 interference, can be formed:

$$\hat{\varepsilon}\cdot\vec{E}\ \hat{k}\times\hat{\varepsilon}\cdot\vec{J} \tag{86}$$

$$\hat{\varepsilon}\cdot\vec{J}\ \hat{k}\times\hat{\varepsilon}\cdot\vec{E} \tag{87}$$

Figure 16 gives the orientation of the various vectors. Choosing $\hat{k}$ along $\hat{x}$, $\vec{E}$ along $\hat{y}$, and $\hat{\varepsilon}$ along $\hat{y}$, we find that expression (86) permits a final polarization along z, which reverses sign with $\hat{k}$ and $\vec{E}$. Such a polarization actually occurs in the transitions (Cs, $6^2S_{\frac{1}{2}} \rightarrow 7^2S_{\frac{1}{2}}$) and (Tℓ, $6^2P_{\frac{1}{2}} \rightarrow 7^2P_{\frac{1}{2}}$) for $\Delta F = 0$; $m_F = 0$; for example in Tℓ, the so-called "α" transition $F = 1 \rightarrow F' = 1$, $\Delta m_F = 0$. If $\hat{\varepsilon}$ is along $\hat{z}$ instead, one again has a polarization along z which reverses sign with $\hat{k}$ and $\vec{E}$. This occurs, for example, in the so-called "β" transition $F = 0 \rightarrow F = 1$ in Tℓ, ($\Delta m_F = \pm 1$). Detection of such polarizations by observations of the circular polarization of decay fluorescence yielded measurements

of $\mathcal{H}$ in Cs (Bouchiat & Pottier 1976a) and in Tℓ (Chu et al 1977).

If circularly polarized light is employed, with helicity h = ±1, one can form the T-invariant pseudoscalar

$$h\hat{k}\times\vec{E} \cdot \vec{J} \qquad (88)$$

which represents $\mathcal{E}_p$-Stark interference. With $\hat{k}$ along $\hat{x}$, $\vec{E}$ along $\hat{y}$, $\hat{\varepsilon} = (\hat{y} \pm i\hat{z})/\sqrt{2}$, expression (88) yields a polarization in the z direction which reverses with h and $\vec{E}$, but is independent of the sign of $\hat{k}$. Both the Paris and Berkeley experiments utilize this effect.

At Paris, a CW ring dye laser is employed to excite a single hyperfine component in the 5395 Å transition (Cs, $6^2S_{\frac{1}{2}} \rightarrow 7^2S_{\frac{1}{2}}$). The laser light is circularly polarized with a Pockels cell. It then enters a cesium cell, where it is reflected back and forth about 100 times by a pair of curved mirrors inside the cell. This "multipass" design has two advantages: It amplifies the signal, and at the same time essentially eliminates the polarization caused by the M1-$E_{Stark}$ interference, since this reverses with $\hat{k}$.

The static electric field is maintained with plane parallel electrodes inside the cell. The 7S → 6P fluorescence at 1.36μ is collected and collimated by a lens, passes through an interference filter and circular polarization analyzer, and is then focused onto a germanium detector. The laser polarizer and fluorescence analyzer are both modulated, and lock-in detection techniques are used to extract the parity-violating signal. Background is chiefly due to black-body radiation at 1.36μ from the oven and cell, and a Stark field of ~ 300 V/cm is required to produce a signal large enough for convenient use.

In the Tℓ, $6^2P_{\frac{1}{2}} \rightarrow 7^2P_{\frac{1}{2}}$ experiment (see Figure 16), the transition wavelength of 2927 Å is produced by nonlinear second harmonic generation from the output of a flashlamp-pumped pulsed dye laser tuned to 5854 Å. The light is circularly polarized by passing it through a crystalline quartz quarter-wave plate capable of producing circularly polarized light of great purity (intensity of unwanted polarization $\lesssim 10^{-4}\times$ intensity of wanted polarization). The light then enters the quartz thallium cell, which is in an oven heated to 750-800°C. Oven and cell are inside a rough vacuum, and the cell itself is connected to an ultra-high vacuum system, which is employed to reduce molecular backgrounds due to contaminants. Technical difficulties have prevented using a multipass system; the laser beam either makes a single pass, or makes one reflection and returns. At best, this only reduces the M1 polarization by 78%. $\vec{E}$ is produced by plane parallel electrodes either inside or outside the cell. The $F = 0 \rightarrow F = 1$ transition is used for all parity data. However, the 2.13 GHz hyperfine splitting of the $7^2P_{\frac{1}{2}}$ state is easily resolved, and so it is possible to tune to the $F = 0 \rightarrow F' = 0$ line. In this case, there is no final state polarization; the $0 \rightarrow 0$ line is thus used for a null experiment.

In thallium the polarization of the $7^2P_{\frac{1}{2}}$ state is not easily analyzed by observation of circular polarization of decay fluorescence. Black-body radiation prevents viewing the 1.3μ $7P_{\frac{1}{2}} \rightarrow 7S_{\frac{1}{2}}$ transition, and the 5350 Å $7S_{\frac{1}{2}} \rightarrow 6P_{3/2}$ light has only one-twelfth the original polarization. Instead, a second laser is utilized. It drives an optical parametric oscillator which produces photons circularly polarized along the z axis and tuned to the 2.18μ $7P_{\frac{1}{2}} \rightarrow 8S_{\frac{1}{2}}$ E1 transition.

By selective excitation of the $7P_{\frac{1}{2}}$ $F = 1$, $m_F = +1$ or $-1$ states to $8^2S_{\frac{1}{2}}$, and by observation of the $8^2S_{\frac{1}{2}} \rightarrow 6^2P_{3/2}$ fluorescence, the analyzing power of the $7^2P_{\frac{1}{2}}$ polarization is about 70%. The chief source of background in the thallium experiment is UV fluorescence from the cell scattered into the detectors at the wavelength 3230 Å corresponding to the $8^2S_{\frac{1}{2}} \rightarrow 6^2P_{3/2}$ transition. Signals appreciably greater than background are achieved for a Stark field of 170 V/cm or more.

In order to eliminate laser fluctuations, two separate interaction regions are used, which have opposite handedness for each laser pulse. This is accomplished by splitting the 2.18μ beam and polarizing the two halves oppositely in the two regions. Thus the polarization asymmetry can be measured on each pulse. In addition to reversing the UV $\lambda/4$ plate on successive pulses, the IR polarization and the electric field directions are also reversed periodically. All of these reversals, plus the 0-0 null experiment, reduce possible systematic errors to acceptable levels. The most critical reversal is the UV polarization, which is needed to cancel the M1 asymmetry. By contrast, in the cesium experiment the multipass cell eliminates the M1, but the extremely small size of the expected effect makes the electric field reversal critical. For instance, if the laser beam in either experiment is misaligned so that small components of $\vec{E}$ exist along $\hat{x}$ (the beam direction) and $\hat{z}$, there will be a Stark effect polarization along $\hat{z}$ of $\mathcal{P} = 2E_xE_z/E^2$ which mimics the parity effect. (This is described by the scalar invariant $h\ \vec{J}\cdot\vec{E}\ \hat{k}\cdot\vec{E}$.) The result of the Berkeley experiment (Conti et al 1979) is $\delta = (5.2 \pm 2.4) \times 10^{-3}$, which yields $Q_W = -280 \pm 140$.

Alternative versions of these experiments with attractive features have been considered independently by Bouchiat et al (1979) and Commins (Bucksbaum 1979) and are being carried out. Here one employs linearly polarized light and selects the $m_F$ components of the final state by using an external magnetic field to split Zeeman components. The pseudoscalar of interest is now proportional to

$$\hat{\varepsilon}\cdot\vec{B}\ \hat{\varepsilon}\cdot\vec{E}\times\vec{B}$$

and $\hat{k}$ is chosen $\|$ to E. In this version of the experiment, possible systematic errors arising from circularly polarized light are eliminated, and expected signals in the Tℓ case are much larger than previously attained.

MISCELLANEOUS EFFECTS There should also exist effects in atoms due to the parity-violating neutral weak electron-electron interaction (Bouchiat & Bouchiat 1974b, Sushkov & Flambaum 1978a), but these are expected to be reduced relative to effects due to $H_W^{(1)}$ by a factor of order $Z^{-1}(1 - 4\sin^2\theta)$ in heavy atoms; that is, comparable to effects due to $H_W^{(2)}$ (Novikov et al 1977). Additional modifications arise from radiative corrections to $H_p$ (Marciano & Sanda 1978).

Parity violation effects in diatomic molecules have been discussed by Sushkov & Flambaum (1978b); and Rein et al (1979) have considered parity-violating energy differences between mirror-image molecules and have found them to be very small. Other aspects of the latter question have been considered by Harris & Stodolsky (1978). Possible manifestations of parity violation in the Josephson effect have been discussed by Vainshtein & Khriplovich (1974, 1975).

## 5. SUMMARY AND CONCLUSIONS

The results of electron scattering and atomic physics experiments (eq sector) may be combined with neutrino-nucleon (νq) and neutrino-electron (νe) scattering data to provide a stringent test of neutral weak interaction theories. In carrying out this analysis it is useful to begin with the simplest possible model-independent assumptions (Hung & Sakurai 1979, Sakurai 1979). Thus we start merely by assuming μe universality, that the contributions of heavy quarks c,s,... may be neglected, and that all neutral weak currents possess only vector and axial vector components. We may then write the effective Hamiltonians:

$$H_{\nu q} = -\frac{G}{\sqrt{2}}\bar{\nu}\gamma_\lambda(1-\gamma_5)\nu\{\tfrac{1}{2}[\bar{u}\gamma_\lambda(\alpha-\beta\gamma_5)u - \bar{d}\gamma_\lambda(\alpha-\beta\gamma_5)d] + \tfrac{1}{2}[\bar{u}\gamma_\lambda(\gamma-\delta\gamma_5)u + \bar{d}\gamma_\lambda(\gamma-\delta\gamma_5)]\}; \quad (89)$$

$$H_{\nu e} = -\frac{G}{\sqrt{2}}[\bar{\nu}_\mu\gamma_\lambda(1-\gamma_5)\nu_\mu][e(g_V\gamma_\lambda - g_A\gamma_\lambda\gamma_5)e]; \quad (90)$$

$$H_{eq} = -\frac{G}{\sqrt{2}}\{e\gamma_\lambda\gamma_5 e[\frac{\tilde{\alpha}}{2}(\bar{u}\gamma_\lambda u - \bar{d}\gamma_\lambda u) + \frac{\tilde{\gamma}}{2}(\bar{u}\gamma_\lambda u + d\gamma_\lambda d)] + \bar{e}\gamma_\lambda e[\frac{\tilde{\beta}}{2}(\bar{u}\gamma_\lambda\gamma_5 u - \bar{d}\gamma_\lambda\gamma_5 d) + \frac{\tilde{\delta}}{2}(\bar{u}\gamma_\lambda\gamma_5 u + \bar{d}\gamma_\lambda\gamma_5 d)]\}. \quad (91)$$

The ten coupling constants $\alpha,\beta,\ldots\tilde{\beta},\tilde{\delta}$ must be determined by experiment. Note that Eq. (91) reduces to Eqs. (4), (5) provided we put

$$C_{1p} = -\tfrac{1}{2}(3\tilde{\gamma} + \tilde{\alpha}), \quad C_{1n} = -\tfrac{1}{2}(3\tilde{\gamma} - \tilde{\alpha}),$$

which follow from the assumption that p = 2u+d, n = 2d+u.

The neutrino-nucleon scattering data yield values of $\alpha,\beta,\gamma$, and $\delta$ which are determined up to an overall sign ambiguity. These are listed in Table 6, column 1. For a review of neutrino-scattering, see Cline &

Fry 1977). Note that $\beta$ is determined from a recent measurement of the cross section for

$$\bar{\nu}_e + D \to \bar{\nu}_e + n + p \tag{92}$$

in which low-energy electron-antineutrinos are employed (Pasierb et al 1979). In $\bar{\nu}_e + e \to \bar{\nu}_e + e$ charged and neutral currents can participate. All other neutrino scattering experiments have so far utilized high energy $\nu_\mu$ or $\bar{\nu}_\mu$.

The coupling constants $g_V, g_A$ for $\nu e$ scattering have now been measured to be:

$$\begin{aligned} g_A &= -0.52 \pm 0.06 \\ g_V &= .06 \pm .08. \end{aligned} \tag{93}$$

Actually there is an ambituity involving $g_A \leftrightarrow g_V$ here; we have written the "axial vector dominant" solution.

Next, the results of the SLAC electron scattering experiment are expressed in terms of the coefficient $a_1$, $a_2$ appearing in $\Delta/(-q^2)$ [Eq. (52)].

Writing

$$a_1 = \frac{G}{\sqrt{2}\, e^2} \frac{9\tilde{\alpha} + 3\tilde{\gamma}}{5} \tag{94}$$

$$a_2 = \frac{G}{\sqrt{2}\, e^2} \frac{9\tilde{\beta} + 3\tilde{\delta}}{5} \tag{95}$$

and recalling the experimental values for $a_{1,2}$ [Eqs. (58) (59)], we find:

$$\tilde{\alpha} + \frac{\tilde{\gamma}}{3} = -0.60 \pm 0.16 \tag{96}$$

$$\tilde{\beta} + \frac{\tilde{\delta}}{3} = 0.31 \pm 0.51. \tag{97}$$

The results of the Novosibirsk and Berkeley Tℓ and Bi experiments: $Q_W(Bi) = -140 \pm 40$ and $Q_W(T\ell) = -280 \pm 140$ are expressible in terms of $\tilde{\alpha}$ and $\tilde{\gamma}$ by means of the relation:

$$Q_W = -e\tilde{\gamma}(Z+N) + \tilde{\alpha}(Z-N). \tag{98}$$

We plot the experimental constraints on $\tilde{\alpha}$ and $\tilde{\gamma}$ in Figure 17. Thus we obtain:

$$\tilde{\alpha} = -0.72 \pm 0.25 \tag{99}$$

$$\tilde{\gamma} = .38 \pm 0.28. \tag{100}$$

Further restrictions on the coupling constants are obtained if one assumes a model with single Z boson exchange (the "factorization" hypothesis). Assuming μe universality, this is characterized by seven independent parameters for coupling Z to $\nu_L$, $u_{L,R}$, $d_{L,R}$, and $e_{L,R}$. Since we started with ten parameters $\alpha, \beta, \ldots \bar{\delta}$ there must be three independent "factorization" relations connecting the latter. Hung & Sakurai (1977) have shown these to be

$$\tilde{\gamma}/\tilde{\alpha} = \gamma/\alpha \tag{101}$$

$$\tilde{\delta}/\tilde{\beta} = \delta/\beta \tag{102}$$

$$g_V/g_A = \alpha\tilde{\beta}/\tilde{\beta}\alpha. \tag{103}$$

Let us plot the allowed values of $\gamma/\alpha$ from νq data (Table 6) on Figure 17 and utilize Eq. (101). Then we see that the SLAC and Bi,Tℓ results fall within the region permitted by νq data; this provides model-independent evidence for factorization.

Since $\tilde{\beta}$ and $\tilde{\delta}$ have not yet been separately determined (this would require a measurement of parity violation at the $\beta_o e_o$ crossing in hydrogen, for example), one cannot test Eq. (102) directly. However, combining Eqs. (101), (102), and (103), one obtains:

$$g_V/g_A = \frac{[\alpha + (\gamma/3)][\beta + (\delta/3)]}{[\tilde{\alpha} + (\tilde{\gamma}/3)][\tilde{\beta} + (\tilde{\delta}/3)]} . \qquad (104)$$

From the experimentally determined ratio $a_2/a_1$ [Eqs. (96) and (97)] one can determine the right hand side of Eq. (104). This determines that only the "axial-vector dominant" solution for $g_V, g_A$ is acceptable in νe scattering, as we have written in Eq. (93).

One may make use of the SLAC experimental result [Eqs. (96),(97)] and the factorization condition [Eq. (102)], with $\delta/\beta$ determined from νq data (Table 7) to obtain:

$$\tilde{\beta} = 0.29 \begin{smallmatrix} +0.55 \\ -0.51 \end{smallmatrix}$$
$$\tilde{\delta} = 0.02 \begin{smallmatrix} +0.17 \\ -0.06 \end{smallmatrix} . \qquad (105)$$

Another factorization relation:

$$\begin{Bmatrix} \tilde{\beta} \\ \tilde{\delta} \end{Bmatrix} = \begin{Bmatrix} \beta \\ \delta \end{Bmatrix} \frac{g_V}{g_A} \frac{\tilde{\alpha} + (\tilde{\gamma}/3)}{\alpha + (\gamma/3)} \qquad (106)$$

yields more precise limits:

$$\tilde{\beta} = 0.06 \pm 0.21$$
$$\tilde{\delta} = 0.00 \pm 0.02 \qquad (107)$$

Now, the signs of the $\bar{\nu}_e e$ coupling constants $g_V, g_A$ can be determined experimentally, since the neutral-current and charged-current amplitudes interfere. (We make a standard V-A choice of sign for the latter.) Also, the signs of the eq constants $\tilde{\alpha}, \tilde{\beta}, \tilde{\gamma}, \tilde{\delta}$ are determined because of interference with the electromagnetic amplitude of known sign. One cannot measure directly the absolute sign of νq coupling constants. However, it can be shown (Sakurai 1979) that the factorization hypothesis, together with the assumption that the coupling strength $c_\nu^2$ in $\nu + \nu \to \nu + \nu$ is positive, removes the sign ambiguity in the νq constants.

Table 6 column 2 gives the present values of the ten coupling parameters which are thus obtained. The Weinberg-Salam model predictions of these parameters are also given in Table 6, column 3, and it is clear that very satisfactory agreement is obtained for $\sin^2\theta = 0.23$ (column 4). However, it is obviously desirable and important to improve the precision of determination of the parameters, especially $\gamma, \delta, \tilde{\beta}, \tilde{\gamma}$ and $\tilde{\delta}$. Better values of $\tilde{\gamma}$ will soon be obtained from heavy atom experiments, and $\tilde{\beta}$, $\tilde{\gamma}$, and $\tilde{\delta}$ may be measured accurately in hydrogen atom experiments within the next few years. Beyond this one may hope that various experiments will eventually shed light on small but important effects such as the electron-electron parity violating coupling, momentum-transfer dependent terms and higher order corrections to the Weinberg-Salam model. The latter would be particularly exciting to observe since the ability to predict them is one of the most important features of unified gauge field theories.

We are grateful to the following persons for providing us with materials related to their work before publication: Drs. M.A. Bouchiat and L. Pottier, Prof. C. Bouchiat, Prof. E. Adelberger, Prof. E. Hinds, Dr. C. Prescott, Prof. P.G.H. Sandars, Prof. J.J. Sakurai, and Prof. W. Williams. We also thank them and Profs. E.N. Fortson, I.B. Khriplovich and V. Telegdi for helpful discussions. This review was written under the auspices of the Chemical Sciences Division, Office of Basic Energy Sciences, U.S. Department of Energy.

Literature Cited

Abers, E.S., Lee, B.W. 1973. Phys. Rep. Phys. Lett. C. 9C:1-141

Baird, P.E.G., Brimicombe, M.W.S.M., Hunt, R.G., Roberts, G.J., Sandars, P.G.H., Stacy, D.N. 1977. Phys. Rev. Lett. 39: 98-801

Barkov, L.M., Zolotorev, M.S. 1978a. Pis'ma Zh. Eksp. Teor. Fiz. 27:379-83 (JETP Lett. 27:357-61)

Barkov, L.M., Zoltorev, M.S. 1978b. Pis'ma Zh. Eksp. Teor. Fiz. 28:544-48 (JETP Lett. 28:503-6)

Barkov, L.M., Zolotorev, M.S. 1979. Phys. Lett. 85B:308-13

Bell, J.S. 1979. Proc. Workshop Parity Violation in Atoms, Cargese, Corsica, September 1979, in press

Bjorken, J.D., Drell, S.D. 1964. Relativistic Quantum Mechanics, New York: McGraw-Hill.

Bouchiat, C. 1975. Phys. Lett. 57B: 284-88

Bouchiat, M.A., Bouchiat, C. 1974a. Phys. Lett. 48B:111-14

Bouchiat, M.A., Bouchiat, C. 1974b. J. Phys. (Paris) 35:899-927

Bouchiat, M.A., Bouchiat, C. 1975. J. Phys. (Paris) 36:493-509

Bouchiat, M.A., Poirier, M., C. Bouchiat. 1979. In press

Bouchiat, M.A., Pottier, L. 1976a. J. Phys. Lett. (Paris) 37: L79-L83

Bouchiat, M.A., Pottier, L. 1976b. Phys. Lett. 62B:327-30

Bouchiat, M.A., Pottier, L. 1979. See Bell, 1979. In press

Brimicombe, M.W.S.M., Loving, C.E., Sandars, P.G.H. 1976. J. Phys. B9:L237-40

Bucksbaum, P.H. 1979. See Bell, 1979. In press

Cahn, R.N., Gilman, F.J. 1978. Phys. Rev. D. 17:1313-22

Carter, S.L., Kelley, H.P. 1979. Phys. Rev. Lett. 42:966-69

Chu, S., Commins, E.D., Conti, R. 1977. Phys. Lett. 60A;96-100

Cline, D., Fry, W. 1977. Ann. Rev. Nucl. Sci. 27: 209-78

Conti, R., Bucksbaum, P., Chu, S., Commins, E., Hunter, L. 1979. Phys. Rev. Lett. 42:343-46

Dunford, R.W., Lewis, R.R., Williams, W.L. 1978. Phys. Rev. A. 18:2421-36

Englert, F., Brout, R. 1964. Phys. Rev. Lett. 13:321-23

Feynmann, R.P., Gell-Mann, M. 1958. Phys. Rev. 109:193-98

Flambaum, V.V., Khriplovich, I.B., Sushkov, O.P. 1978. Phys. Lett. 67A:177-79

Glashow, S.L., Iliopoulos, J., Maiani, L. 1970. Phys. Rev. D. 2:1285-92

Grant, I.P., Rose, S.J., Sandars, P.G.H. 1979. In press

Goldstone, J. 1961. Nuovo Cimento 19:154-64

Goldstone, J., Salam, A., Weinberg, S. 1962. Phys. Rev. 127:965-70

Gould, H. 1970. Phys. Rev. Lett. 24:1091-93

Guralnik, G.S., Hagen, C.R., Kibble, T.W.B. 1964. Phys. Rev. Lett. 13:585-87

Harris, M.J., Loving, C.E., Sandars, P.G.H. 1978. J. Phys. B. 11:L749-53

Harris, R.A., Stodolsky, L. 1978. Phys. Lett. 78B:313-16

Harrison, G.E., Sandars, P.G.H., Wright, S.J. 1969. Phys. Rev. Lett. 22:163-65

Henley, E.M., Klapisch, M., Wilets, L. 1977. Phys. Rev. Lett. 39:994-97

Henley, E.M., Wilets, L. 1976. Phys. Rev. A. 14:1411-17

Higgs, P.W. 1964a. Phys. Lett. 12:132-33

Higgs, P.W. 1964b. Phys. Rev. Lett. 13:508-9

Higgs, P.W. 1966. Phys. Rev. 145:1156-63

Hiller, J., Sucher, J., Feinberg, G., Lynn, B. 1979. Relativistic Theory of Parity-Violation in Many-Electron Atoms. In press

Hinds, E.A., Loving, C.E., Sandars, P.G.H. 1976. Phys. Lett. 62B:97-99

Hinds, E.A. 1979. See Bell, 1979. In press

't. Hooft, G. 1971. Nucl. Phys. B. 35:167-88

Hung, P.Q., Sakurai, J.J. 1977a. Phys. Lett. 69B:323-38

Hung, P.Q., Sakurai, J.J. 1977b. Phys. Lett. 72B:208-14

Hung, P.Q., Sakurai, J.J. 1979. UCLA Rep. /79/TEP/9 May 1979 Univ. of California, Los Angeles, CA

Khriplovich, I.B. 1974. Pis'ma Zh. Eksp. Teor. Fiz. 20:686-88 (JETP Lett. 20:315-17)

Khriplovich, I.B. 1975. Yad. Fiz. 21:1046 (Sov. J. Nucl. Phys. 21:538-40)

Khriplovich, I.B. 1979. See Bell, 1979. In press

Lee, B.W. 1972. Phys. Rev. D. 5:823-35

Lee, B.W., Zinn-Justin, J. 1972. Phys. Rev. D. 5:3121-60

Lewis, L.L., Hollister, J.H., Soreide, D.C., Lindahl, E.G., Fortson, E.N. 1977. Phys. Rev. Lett. 39:795-98

Loving, C.E., Sandars, P.G.H. 1975. J. Phys. B. 8:L336-38

Marciano, W.J., Sanda, A.E. 1978. Phys. Rev. D. 17:3055-64

Moskalev, A.N. 1974a. Pis'ma Zh. Eksp. Teor. Fiz. 19:229 (JETP Lett. 19:141-50)

Moskalev, A.N. 1974b. Pis'ma Zh. Eksp. Teor. Fiz. 19:394 (JETP Lett. 19:2.6-18)

Neuffer, D.V., Commins, E.D. 1977a. Phys. Rev. A. 16:844-62

Neuffer, D.V., Commins, E.D. 1977b. Phys. Rev. A. 16:1760-67

Novikov, V.N., Sushkov, O.P., Khriplovich, I.B. 1976. Sov. Phys. (JETP) 44:872-80

Novikov, V.N., Sushkov, O.P., Flambaum, V.V., Khriplovich, I.B. 1977. Zh. Eksp. Teor. Fiz. 46:802 (Sov. Phys. JETP 46: 420-22)

Pasierb, E., Gurr, H.S., Lathrop, J., Reines, F., Sobel, H.W. 1979. Phys. Rev. Lett. 43:96-99

Prescott, C.Y., Atwood, W.B., Cottrell, R.L.A., DeStaebler, H., Garwin, E., Gonidec, A., Miller, R.H., Rochester, L.S., Sato, T., Sherden, D.J., Sinclair, C.K., Stein, S., Taylor, R.E., Clendenin, J.E., Hughes, V.W., Sasao, N., Schuler, K.P., Borghini, M.G., Lubelsmeyer, K., Jentschke, W. 1978. Phys. Lett. 77B:347-52

Prescott, C.Y., Atwood, W.B., Cottrell, R.L.A., DeStaebler, H., Garwin, E., Gonidec, A., Miller, R.H., Rochester, L.S., Sato, T., Sherden, D.J., Sinclair, C.K., Stein, S., Taylor, R.E., Clendenin, J.E., Hughes, V.W., Sāsao, N., Schuler, K.P., Borghini, M.G., Lubelsmeyer, K., Jentschke, W. 1979. SLAC Pub. 2319 (1979), SLAC, Palo Alto, CA

Rein, D.W., Hegstron, R.A., Sandars, P.G.H. 1979. Phys. Lett. 71A:499-502

Sakurai, J.J., 1979. UCLA Rep. /79/TEP/1S. Univ. of California, Los Angeles, CA

Salam, A. 1968. In Relativistic Groups and Analyticity (Nobel Symposium #8), ed. N. Svartholm, p. 367. Stockhom: Almqvist and Wiksell

Sandars, P.G.H. 1968. J. Phys. B1:499-510

Sandars, P.G.H. 1975. Atomic Physics IV, pp. 27-35. New York: Plenum.

Sandars, P.G.H. 1979. Many Body Aspects of Parity Non-Conservation in Heavy Atoms. In press

Soreide, D.C., Fortson, E.N. 1975. Bull Am. Phys. Soc. 20:491 (Abstr.)

Sudarshan, E.C.G., Marshak, R. 1958. Phys. Rev. 109:1860-61

Sushkov, O.P., Flambaum, V.V. 1978a. Yad. Fiz. 27:1308 (Sov. J. of Nucl. Phys. 27:690-92)

Sushkov, O.P., Flambaum, V.V. 1978b. Sov. Phys. JETP 75:#10

Sushkov, O.P., Flambaum, Khriplovich, I.B. 1976. Pis'ma Zh. Eksp. Teor. Fiz. 24:502 (JETP Lett. 24:461-64)

Trainor, T. 1979. See Bell, 1979. In press

Vainshtein, A.E., Khriplovich, I.B. 1974. Pis'ma Zh. Eksp. Teor. Fiz. 20:80 (JEPT Lett. 20:34-35)

Vainshtein, A.E., Kriplovich, I.B. 1975. Zh. Eksp. Teor. Fiz. 68:3 (Sov. Phys. JETP 41:1-3)

Weinberg, S. 1967. Phys. Rev. Lett. 19:1264-66

Weinberg, S. 1972. Phys. Rev. D. 5:1412-17

Yang, C.N., Mills, R.N. 1954. Phys. Rev. 96:191-95

Zel'dovich, Ya. B. 1959. Zh. Eksp. Teor. Fiz. 36:964- (Sov. Phys.--JETP 9:682L-683L)

Figure Legends

Figure 1 Feynmann diagrams for photon ($\gamma$) and neutral intermediate boson ($Z^o$) exchange between e and N.

Figure 2 Theoretical asymmetry in scattering of polarized electrons by deuterons, according to various SU(2)×U(1) gauge models, plotted as a function of y. In all models, the leptons and quarks are assigned to left-handed weak isodoublets. Models differ according to assignment of particles to right-handed weak isomultiplets, as indicated. $E_o$ is a hypothetical neutral heavy lepton. $\sin^2\theta = 0.23$ assumed.

Figure 3 Schematic diagram of SLAC polarized electron scattering experiment.

Figure 4 Momentum acceptance, SLAC polarized electron experiment.

Figure 5 Asymmetry data, SLAC polarized electron experiment. Beam polarization is reversed by reorienting polarizing prism from 0° to 90°. (From Prescott et al 1978.)

Figure 6 Observed asymmetry, SLAC polarized electron experiment (discrete points). Dotted curve represents expected energy-dependence of asymmetry due to electron spin precession. (From Prescott et al 1978.)

Figure 7 Experimental asymmetry in scattering of polarized electrons on deuterium (SLAC), as a function of y. ■ : E = 19.4 GeV; ▲ : E = 16.2 GeV; ○ : E = 22.2 GeV. (From Prescott et al 1979.)

Figure 8 Zeeman effect in the hyperfine structure of $2^2S_{\frac{1}{2}}$ and $2^2S_{\frac{1}{2}}$ states of atomic hydrogen. Parity violation causes mixing of levels $\beta_o, e_o$; $\beta_o, f_o$; $\beta_{-1} f_{-1}$.

Figure 9 Schematic diagram of experiment to observe parity violation in hydrogen at Michigan.

Figure 10 (a) Schematic diagram of Yale hydrogen experiment.

(b) Orientation of vectors in the Yale hydrogen experiment. $\vec{\epsilon}_{R1}$, $\vec{\epsilon}_{R2}$ refer to microwave electric fields in regions 1,2 respectively. $\vec{E}_1$ is static electric field, $\vec{B}$ is magnetic field.

Figure 11 Low-lying energy levels of the bismuth atom. Optical rotation experiments have been carried out using the 648 nm and 876 nm transitions.

Figure 12 Energy levels of the cesium atom. The forbidden M1 transition $6^2S_{\frac{1}{2}} \rightarrow 7^2S_{\frac{1}{2}}$ (593 nm) is employed by the Paris group to search for parity violation.

Figure 13 Energy levels of the thallium atom. Parity violation has been observed in the transition $6^2P_{\frac{1}{2}} \rightarrow 7^2P_{\frac{1}{2}}$ (293 nm) at Berkeley.

Figure 14 Novosibirsk optical rotation experiment.

(a) The dashed curve gives the theoretical prediction for parity violating optical rotation vs. wavelength $\lambda$. The solid line is calculated Faraday rotation.

(b) Observed absorption spectrum.

(c) Calculated curve $(1/\ell)d\phi_{PNC}/d\lambda$ and results of measurements of the lines 1,2,3 A. The numbers 6-7, 5-7, etc. refer to hyperfine components F,F'. A is a control line.

Figure 15 Schematic diagrams of optical rotation experiments.

a) Oxford.

b) Novosibirsk.

Figure 16 Schematic diagram of the Berkeley thallium experiment. $L_1, L_2$: Flash-lamp pumped dye lasers. ADA: Nonlinear doubling crystal. LP: linear polarizer. UV $\lambda/4$: 293 nm quarter-wave plate. OPO: Optical parametric oscillator. BS: Beamsplitter. L(R), R(L): reversible 2.18 quarter-wave plates. F: Filters for 323 nm radiation.

Figure 17 Results of the SLAC polarized electron experiment (parameter $a_1$) and the Novosobirsk (Bi) and Berkeley (Tℓ) atomic physics experiments are plotted on the $\tilde{\alpha}$-$\tilde{\gamma}$ plane. The factorization hypothesis together with $\nu$-hadron scattering data constrain the allowed region of the $\tilde{\alpha}$-$\tilde{\gamma}$ plane as shown. (From Sakurai 1979.)

Table 1 Neutral weak interactions

| | neutrino | electron | quark |
|---|---|---|---|
| neutrino | $\nu + \nu \to \nu + \nu$ | $\nu_\mu(\bar{\nu}_\mu) + e \to \nu_\mu(\bar{\nu}_\mu) + e$ (a)<br>$\bar{\nu}_e + e \to \bar{\nu}_e + e$ (b) | $\nu_\mu(\bar{\nu}_\mu) + N \to \nu_\mu(\bar{\nu}_\mu) + X$,<br>$\to \nu_\mu(\bar{\nu}_\mu) + N + \text{Meson}$ } (c)<br>$\to \nu_\mu(\bar{\nu}_\mu) + N$,<br>$\bar{\nu}_e + D \to \bar{\nu}_e + n + p$ (d) |
| electron | | $e + e \to e + e$ (g)<br>$e^+ + e^- \to \mu^+ + \mu^-$ (h) | $e + N \to e + X$ (e)<br>$e + N \to e + N$ (f) |
| quark | | | $N + N \to N + N$ (i)<br>$p + p \to Z + \ldots$ (j)<br>$p + \bar{p} \to Z + \ldots$ |

(Notes to Table 1)

Reaction a - f have been observed.

[a]Scattering of high energy $\nu_\mu(\bar{\nu}_\mu)$ by $e^-$.

[b]Scattering of low energy (reactor) $\bar{\nu}_e$ by $e^-$. This process also occurs by coupling of charged weak currents.

[c]High energy neutrino-nucleon scattering (Cline & Fry 1977).

[d]Low energy reactor $\bar{\nu}_e$ - deuteron scattering (Pasierb 1979).

[e]High energy polarized electron scattering (see Section 3).

[f]Atomic physics (see Section 4).

(Reactions e and f are the subject of this article.)

[g]This reaction can also cause small parity violation effects in atoms.

[h]Interference between photon and $Z^o$ exchange (parity conserving) affects the angular distribution of $\mu^+\mu^-$.

[i]Parity violation in nuclear forces. The charged weak currents also contribute.

[j]Z production in high energy pp, $p\bar{p}$ collisions.

Table 2 Systematic error summary, SLAC polarized electron experiment[a]

| Parameter | Units | Measured Difference (+) - (-) | Correction to $A/-q^2$ |
|---|---|---|---|
| Beam energy | % | $(1.5\pm.28)\times10^{-4}$ | $-.37\times10^{-5}$ |
| Beam current | ma | $(2.2\pm.4)\times10^{-3}$ | -.03 |
| Position parameters | | | |
| x | μ | $(-8.9\pm3.3)\times10^{-2}$ | +.04 |
| y | μ | $(-.65\pm1.8)\times10^{-2}$ | -.02 |
| Beam angle | | | |
| $\theta_x$ | μrad | $(-.37\pm.7)\times10^{-3}$ | .00 |
| $\theta_y$ | μrad | $(1.5\pm.9)\times10^{-3}$ | +.01 |
| Total systematic correction | | | $-.37\times10^{-5}$ |

[a]From Prescott et al (1978).

Table 3 Experimental Parameters for the Hydrogen Experiments

| Experiment | Michigan | Yale |
|---|---|---|
| Transition | $\alpha_o$-$\beta_o$ Stark induced | $\beta_o$-$\beta_-$ Stark induced |
| Magnetic field | 545 g ($\beta_o e_o$ crossing) | 500-600 g |
| PNC mixing | $\beta_o e_o$ | $\beta_o e_o$ |
| Coupling constant | $C_{2p}$ | $C_{2p}$ |
| Pseudoscalar | $(\hat{\varepsilon}\cdot\vec{E})(\hat{\varepsilon}\cdot\vec{B})$ | $(\vec{E}_1\cdot\vec{B})(\hat{\varepsilon}_{R1}\times\vec{B})\cdot(\hat{\varepsilon}_{R2}\times\vec{B})$ or $(\vec{E}_1\cdot\vec{B})(\hat{\varepsilon}_{R1}\times\hat{\varepsilon}_{R2}\cdot\vec{B})$ |
| Size of expected asymmetry for $\sin^2\theta = .23$ | $3 \times 10^{-7}$ | $1.5 \times 10^{-6}$ |
| Expected running time to 1 $\sigma$ | 400 h | 16 h |

Table 4 Calculations of $\mathscr{E}_p$ in bismuth[a] ($\sin^2\theta = .23$ assumed throughout)

| Method | Reference | $\mathrm{Im}(\mathscr{E}_p) \times 10^{10}$ a.u. | |
|---|---|---|---|
| | | $J=3/2 \rightarrow J'=3/2$ | $J=3/2 \rightarrow J'=5/2$ |
| Semi-empirical | (Novikov et al 1976) | -3.24 | .94 |
| Parametric potential | (Harris et al 1978) | -4.16 | 1.31 |
| Parametric potential with shielding | (Harris et al 1978) | -2.78 | .73 |
| Cowan potential (Hartree) | (Henley et al 1977) (Henley & Wilets 1976) | -5.31 | |
| Hartree-Fock length | (Carter & Kelly 1979) | -3.40 | .95 |
| Multiconfiguration Hartree-Fock (MCHF), length[b] | (Grant et al 1979) | -2.82 | 1.32 |
| MCHF, velocity[b] | (Grant et al 1979) | -2.52 | 1.53 |
| HF velocity | (Carter & Kelly 1979) | -2.81 | .13 |

[a] From Sandars (1979a).

[b] 6s and 7s contributions only.

Table 5 Calculations of $\mathscr{E}_p$ and $\delta$ in cesium and thallium ($\sin^2\theta = 0.23$ assumed throughout)

| Element/Transition | Reference | $\mathrm{Im}(\mathscr{E}_p)\times10^{10}$ a.u. | $\delta=2\mathrm{Im}(\mathscr{E}_p)/\mathcal{M}$ |
|---|---|---|---|
| Cs $6^2S_{\frac{1}{2}} \rightarrow 7^2S_{\frac{1}{2}}$ | (Bouchiat & Bouchiat 1974b, 1975) | -0.12 | |
| | (Loving & Sandars 1975, Brimicombe et al 1976) | -0.15 | |
| | (Neuffer & Commins 1977b) | -0.09 | $1.17\times10^{-4}$ |
| Tℓ $6^2P_{\frac{1}{2}} \rightarrow 7^2P_{\frac{1}{2}}$ | (Sushkov et al 1976) | -0.76 | |
| | (Neuffer & Commins 1977a) | -0.83 | $2.2\times10^{-3}$ |
| $6^2P_{\frac{1}{2}} \rightarrow 6^2P_{3/2}$ | (Novikov et al 1976) | -3.3 | |
| | (Neuffer & Commins 1977a) | -3.5 | |
| | (Henley et al 1977, Henley & Wilets 1976) | -4.04, -2.76 | |
| $6^2P_{\frac{1}{2}} \rightarrow 7^2P_{3/2}$ | (Neuffer & Commins 1977a) | + .76 | |

Table 6 Determination of Neutral-Current Coupling Parameters (from Sakurai 1979)

| Parameter | Model-Independent[a] | Factorization Dependent[b] | W-S Model | W-S Model, $\sin^2\theta = 0.23$ |
|---|---|---|---|---|
| $\alpha$ | $\pm 0.58 \pm 0.14$ | $0.58 \pm 0.14$ | $1-2\sin^2\theta$ | 0.54 |
| $\beta$ | $\pm 0.92 \pm 0.14$ | $0.92 \pm 0.14$ | 1 | 1 |
| $\gamma$ | $\mp 0.28 \pm 0.14$ | $-0.28 \pm 0.14$ | $-\frac{2}{3}\sin^2\theta$ | -0.153 |
| $\delta$ | $\pm 0.06 \pm 0.14$ | $0.06 \pm 0.14$ | 0 | 0.0 |
| $g_V$ | $0.00 \pm 0.18$ or $-0.52 \pm 0.13$ | $0.03 \pm 0.12$ | $-\frac{1}{2}(1-4\sin^2\theta)$ | -0.04 |
| $g_A$ | $-0.56 \pm 0.14$ or $-0.07 \pm 0.15$ | $-0.56 \pm 0.14$ | $-\frac{1}{2}$ | -0.5 |
| $\tilde{\alpha}$ | $-0.72 \pm 0.25$ | $-0.72 \pm 0.25$ | $-(1-2\sin^2\theta)$ | -0.54 |
| $\tilde{\beta}$ | --- | $0.06 \pm 0.21$ | $-(1-4\sin^2\theta)$ | -0.08 |
| $\tilde{\gamma}$ | $0.38 \pm 0.28$ | $0.38 \pm 0.28$ | $\frac{2}{3}\sin^2\theta$ | 0.153 |
| $\tilde{\delta}$ | --- | $0.00 \pm 0.02$ | 0 | 0.0 |
| $\tilde{\alpha} + \frac{1}{3}\tilde{\gamma}$ | $-0.60 \pm 0.16$ | $-0.60 \pm 0.16$ | $-(1 - \frac{20}{9}\sin^2\theta)$ | -0.489 |
| $\tilde{\beta} + \frac{1}{3}\tilde{\delta}$ | $0.31 \pm 0.51$ | $0.06 \pm 0.21$ | $-(1-4\sin^2\theta)$ | 0.08 |

[a]Coupling constants determined without recourse to factorization or gauge theory considerations.

[b]Coupling constants determined with factorization constants included.

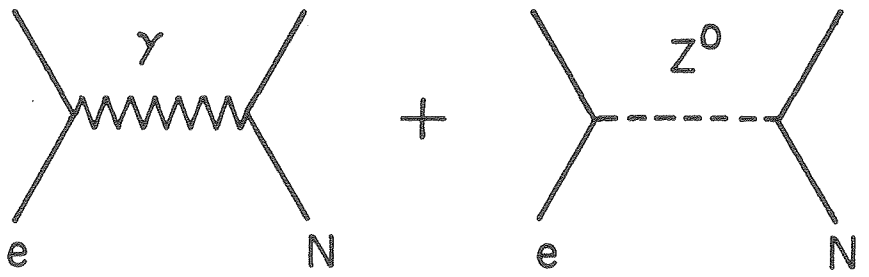


XBL 801-4572

Figure
1

Figure
2

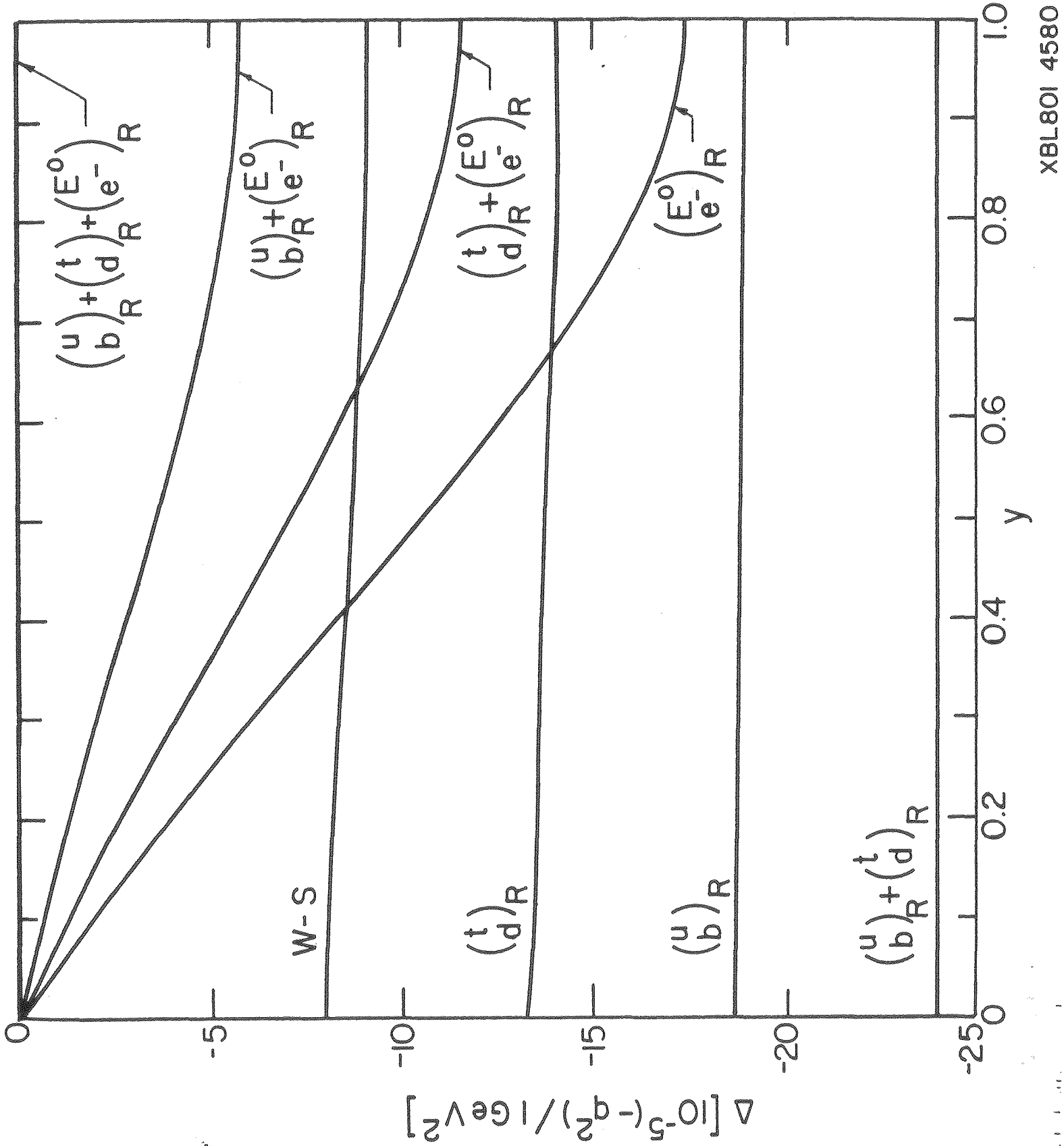
$\left(\begin{matrix}u\\b\end{matrix}\right)_R+\left(\begin{matrix}t\\d\end{matrix}\right)_R+\left(E^0_{e^-}\right)_R$
$\left(\begin{matrix}u\\b\end{matrix}\right)_R+\left(E^0_{e^-}\right)_R$
$\left(\begin{matrix}t\\d\end{matrix}\right)_R+\left(E^0_{e^-}\right)_R$
$\left(E^0_{e^-}\right)_R$
W-S
$\left(\begin{matrix}t\\d\end{matrix}\right)_R$
$\left(\begin{matrix}u\\b\end{matrix}\right)_R$
$\left(\begin{matrix}u\\b\end{matrix}\right)_R+\left(\begin{matrix}t\\d\end{matrix}\right)_R$
0
-5
-10
-15
-20
-25
0
0.2
0.4
0.6
0.8
1.0
y
$\Delta\ [10^{-5}(-q^2)/1\,GeV^2]$
XBL801 4580

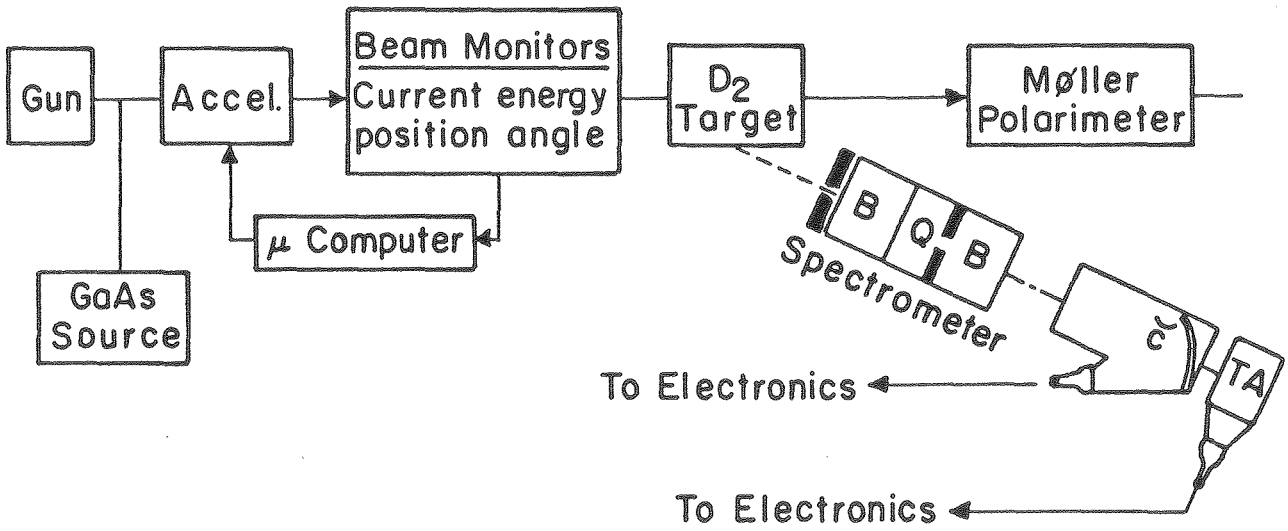
Gun
Accel.
Beam Monitors
Current energy
position angle
D2
Target
Møller
Polarimeter
μ Computer
GaAs
Source
B
Q
B
Spectrometer
c̃
TA
To Electronics
To Electronics
XBL 801-4585

Figure
3

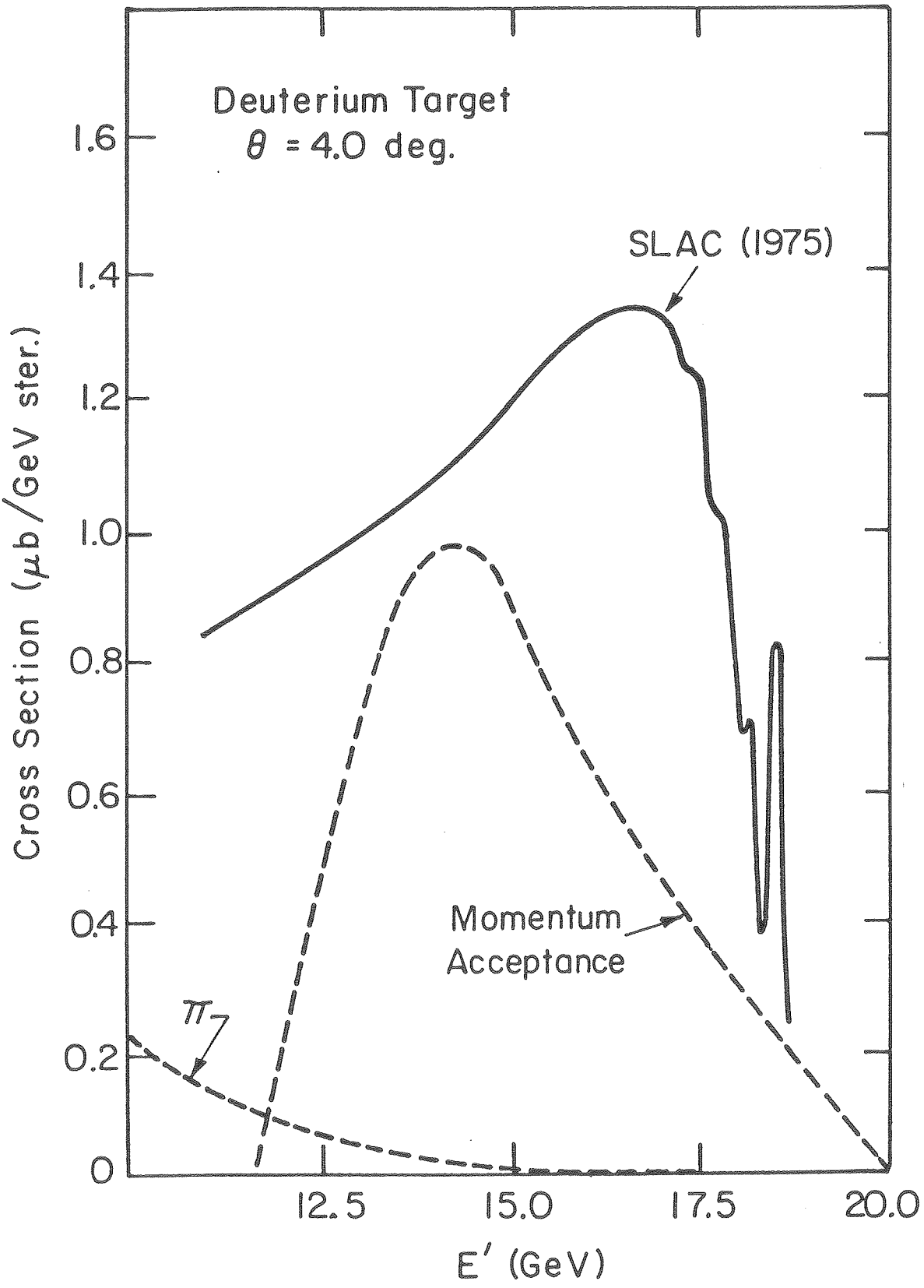


Figure
4

XBL 801-4584

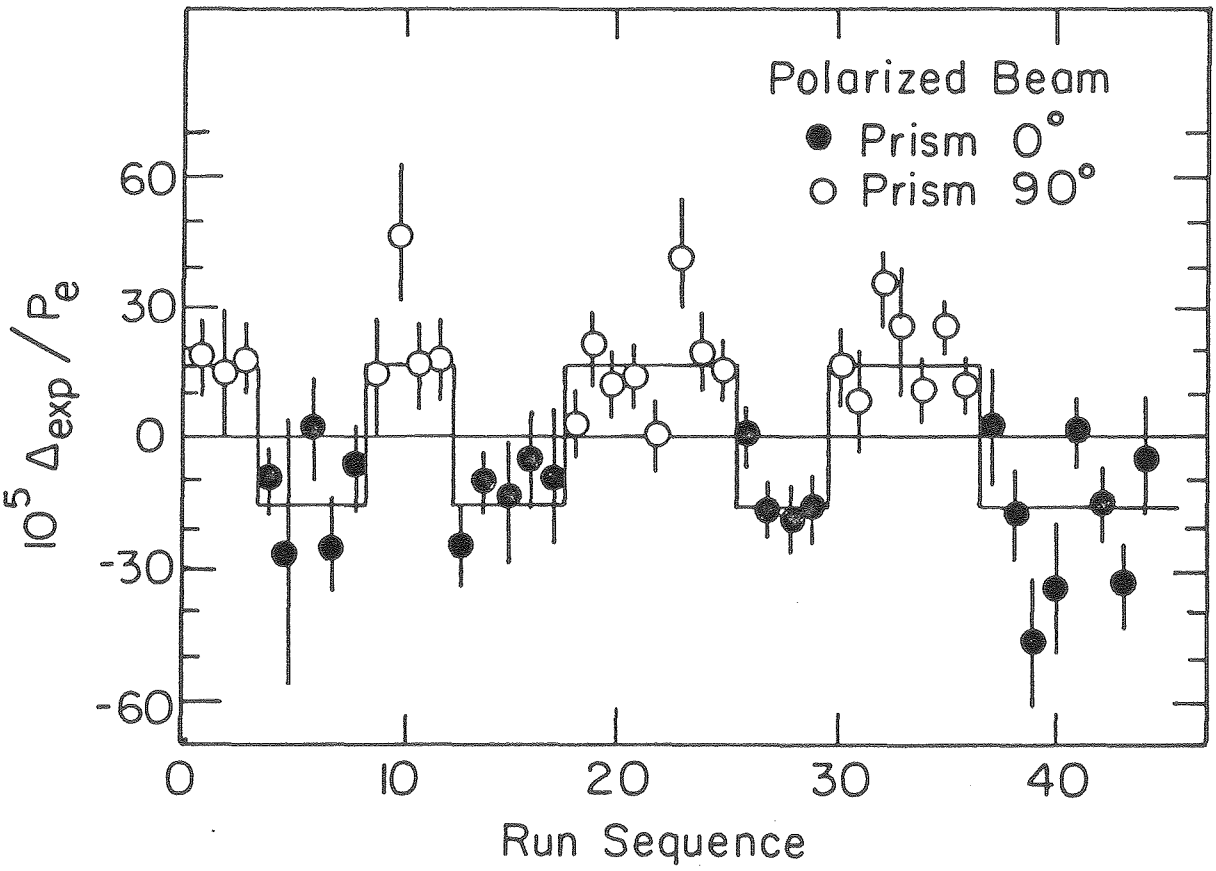


XBL 801-4583

Figure
5

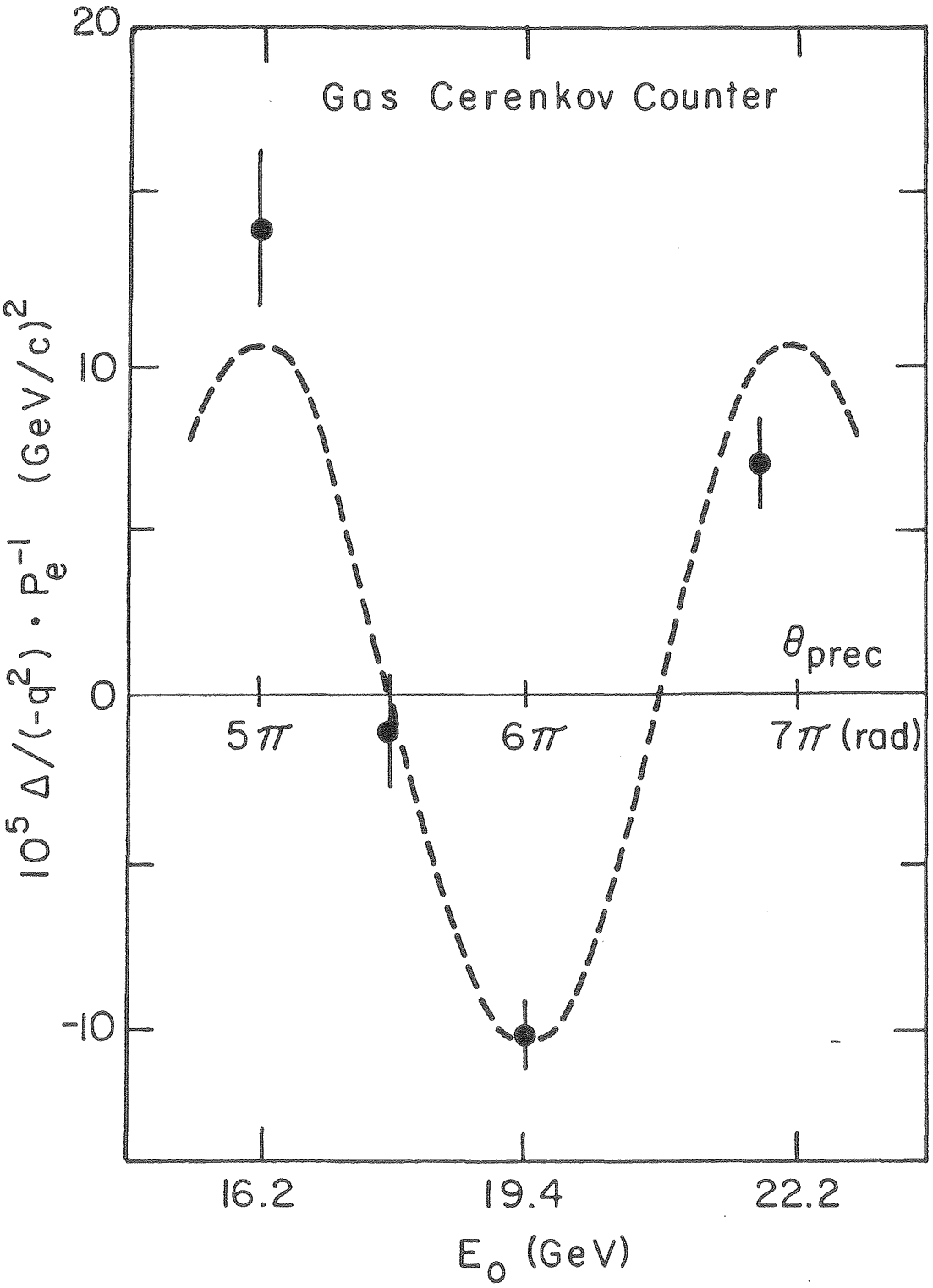


Figure 6

XBL 801-4586

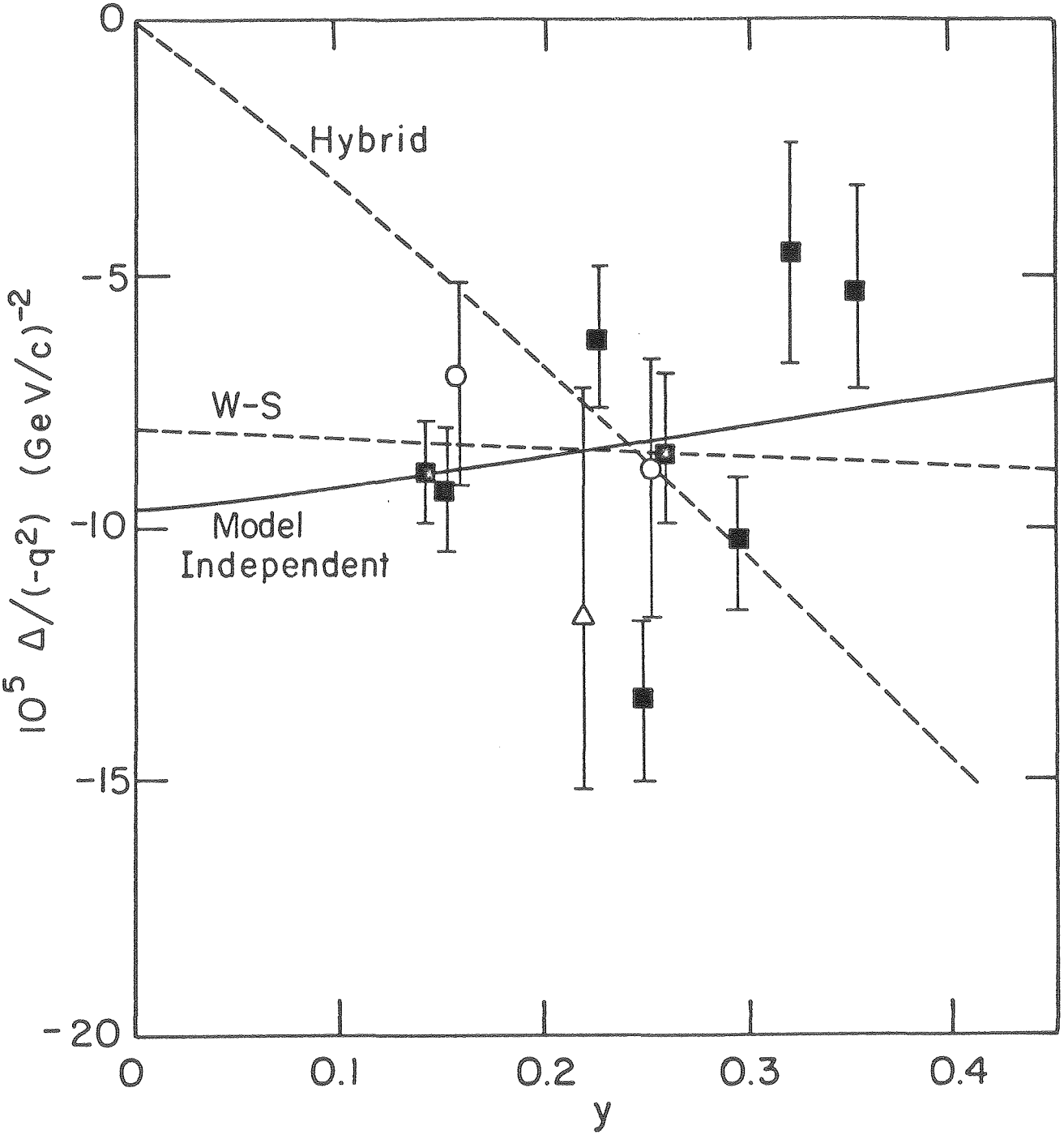


XBL801-4582

Figure
7

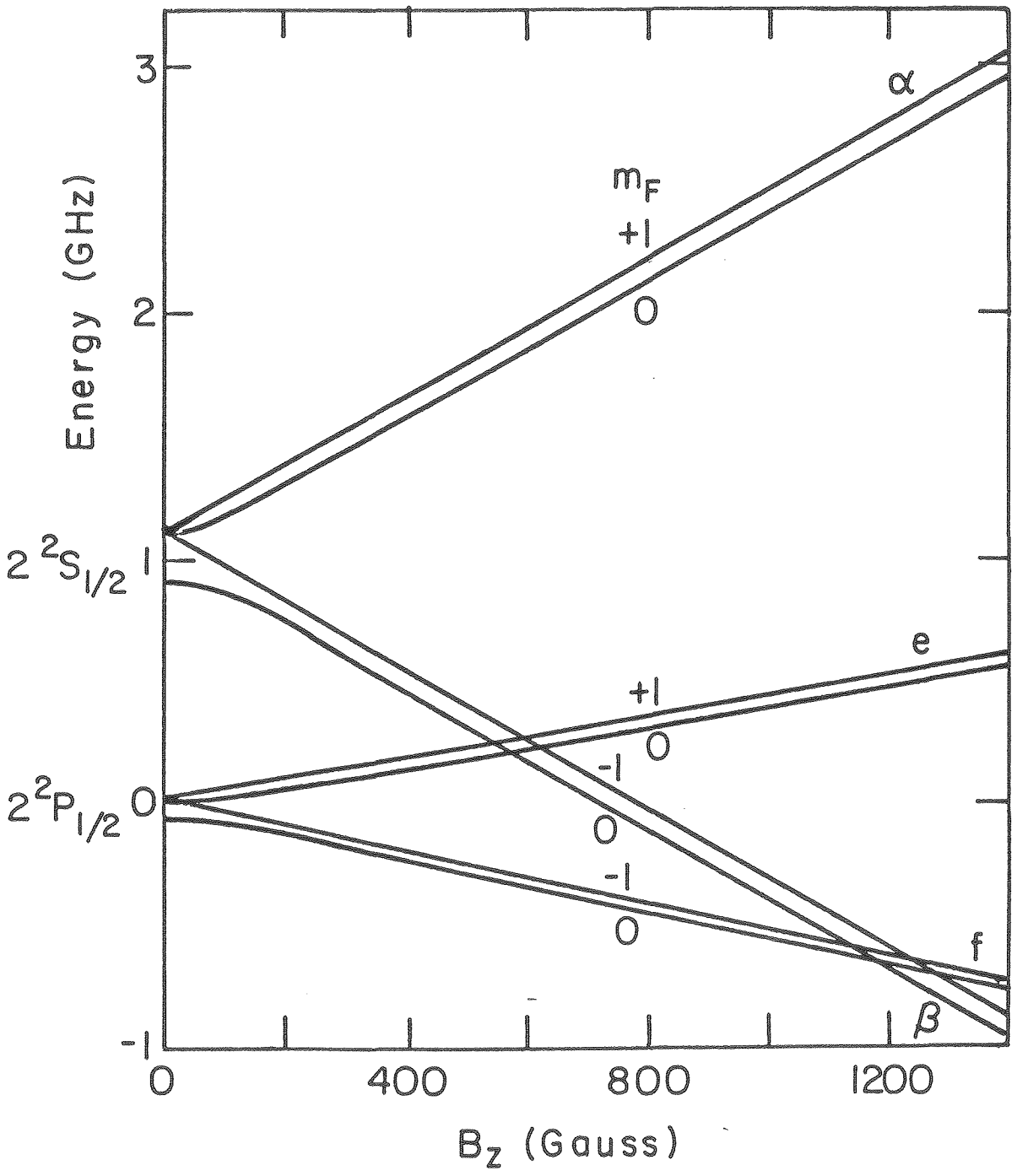


XBL 801-4587

Figure 8

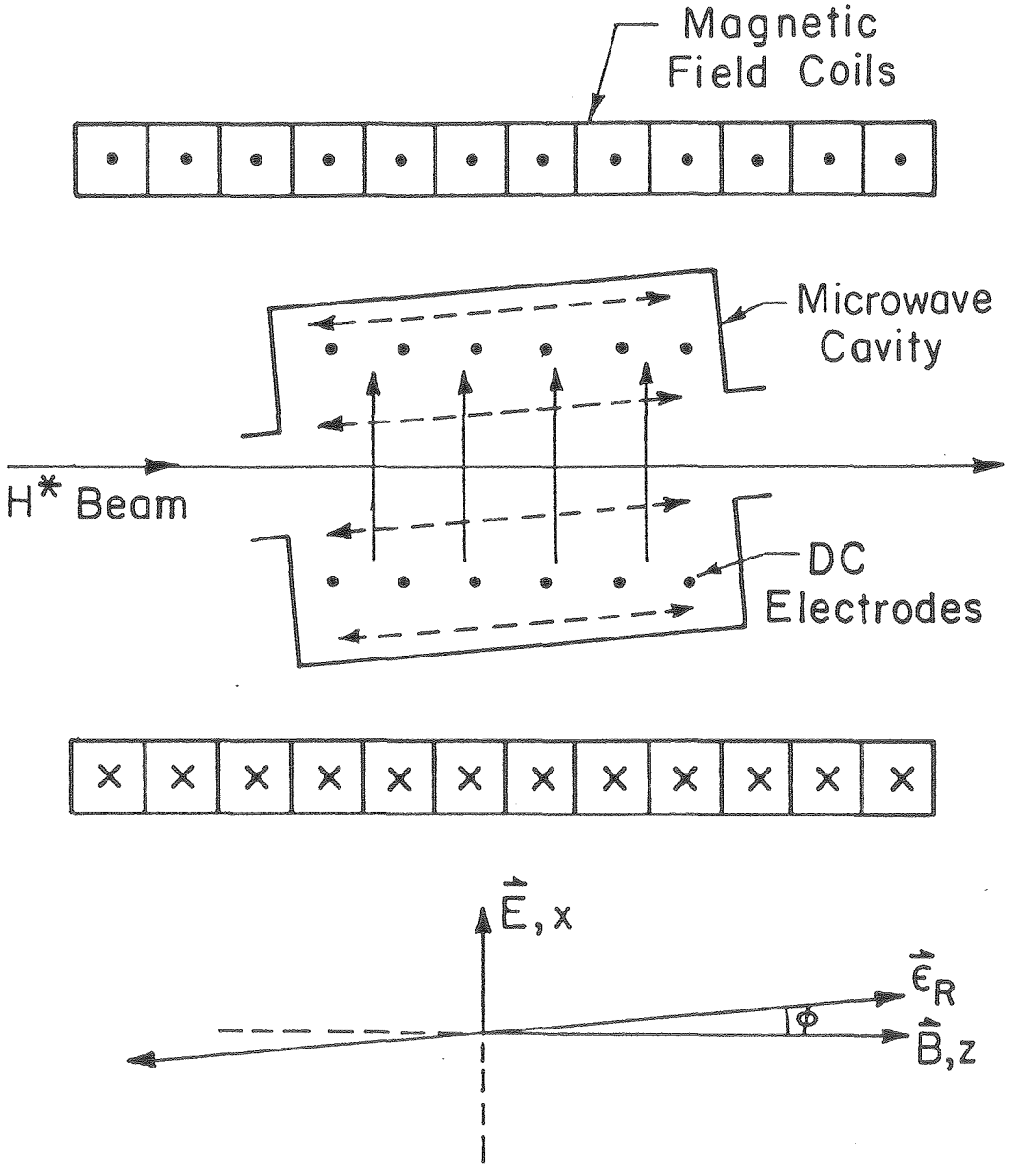


XBL801-4573

Figure
9

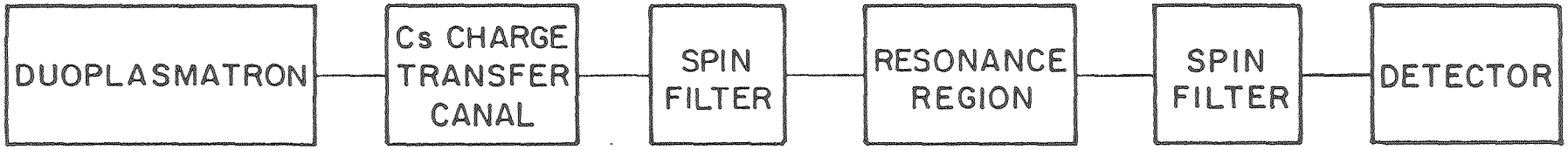


(a)

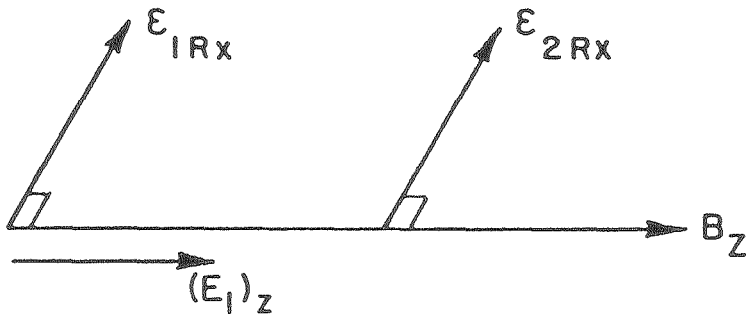


(b)

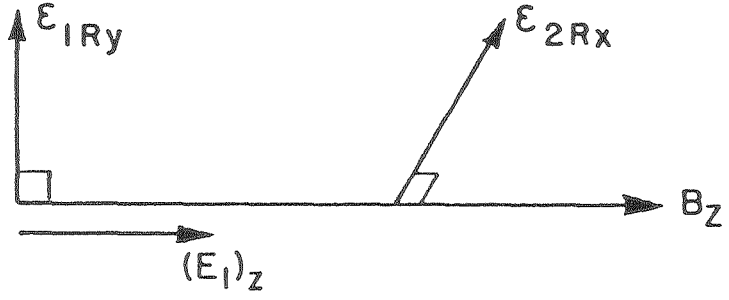


(c)

XBL 801-4579

Figure 10

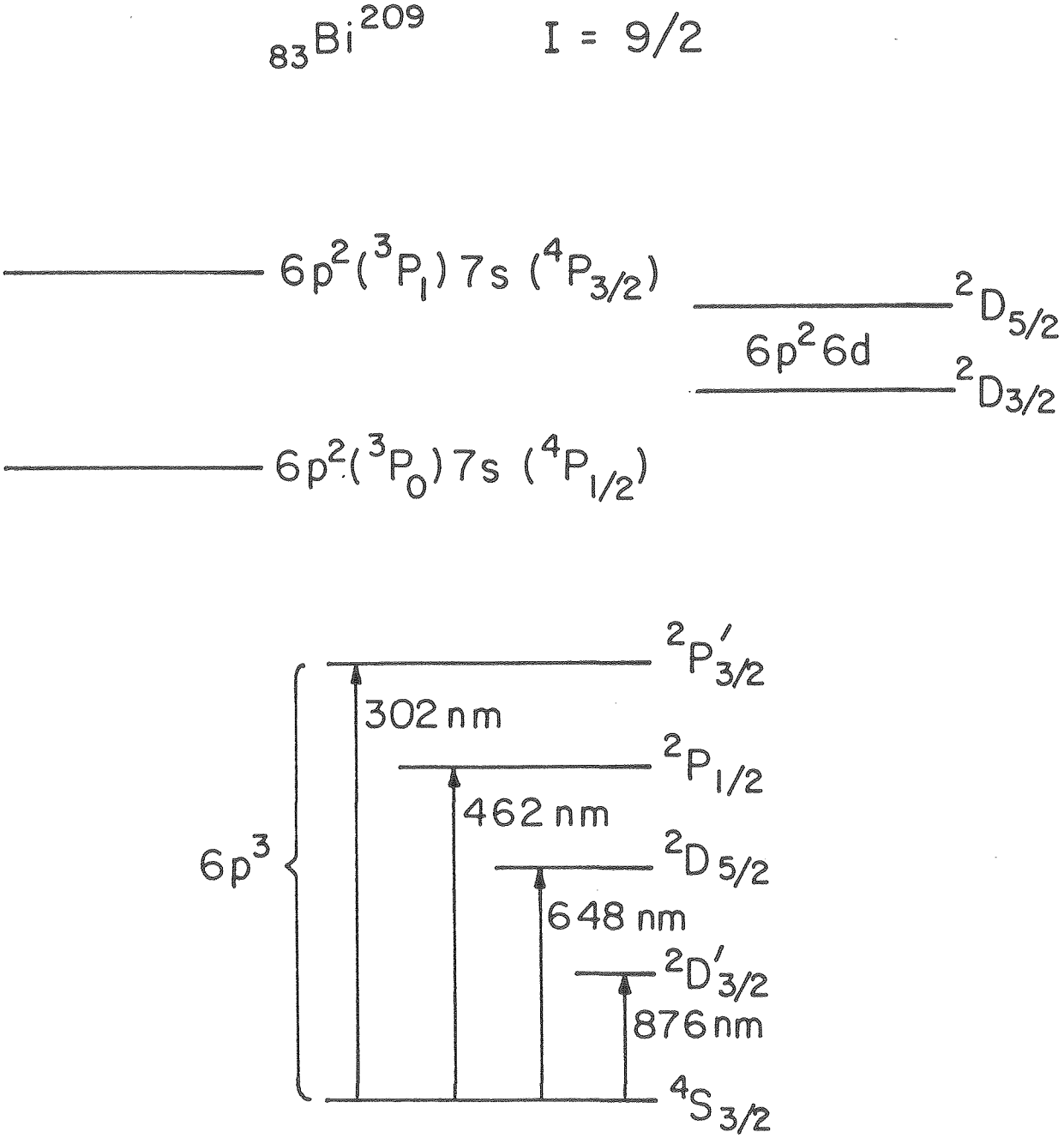
$_{83}Bi^{209}$ I = 9/2
$6p^2(^3P_1)7s\ (^4P_{3/2})$
$^2D_{5/2}$
$6p^2 6d$
$^2D_{3/2}$
$6p^2(^3P_0)7s\ (^4P_{1/2})$
$^2P'_{3/2}$
302 nm
$^2P_{1/2}$
462 nm
$6p^3$
$^2D_{5/2}$
648 nm
$^2D'_{3/2}$
876 nm
$^4S_{3/2}$
XBL 801-4577

Figure
11

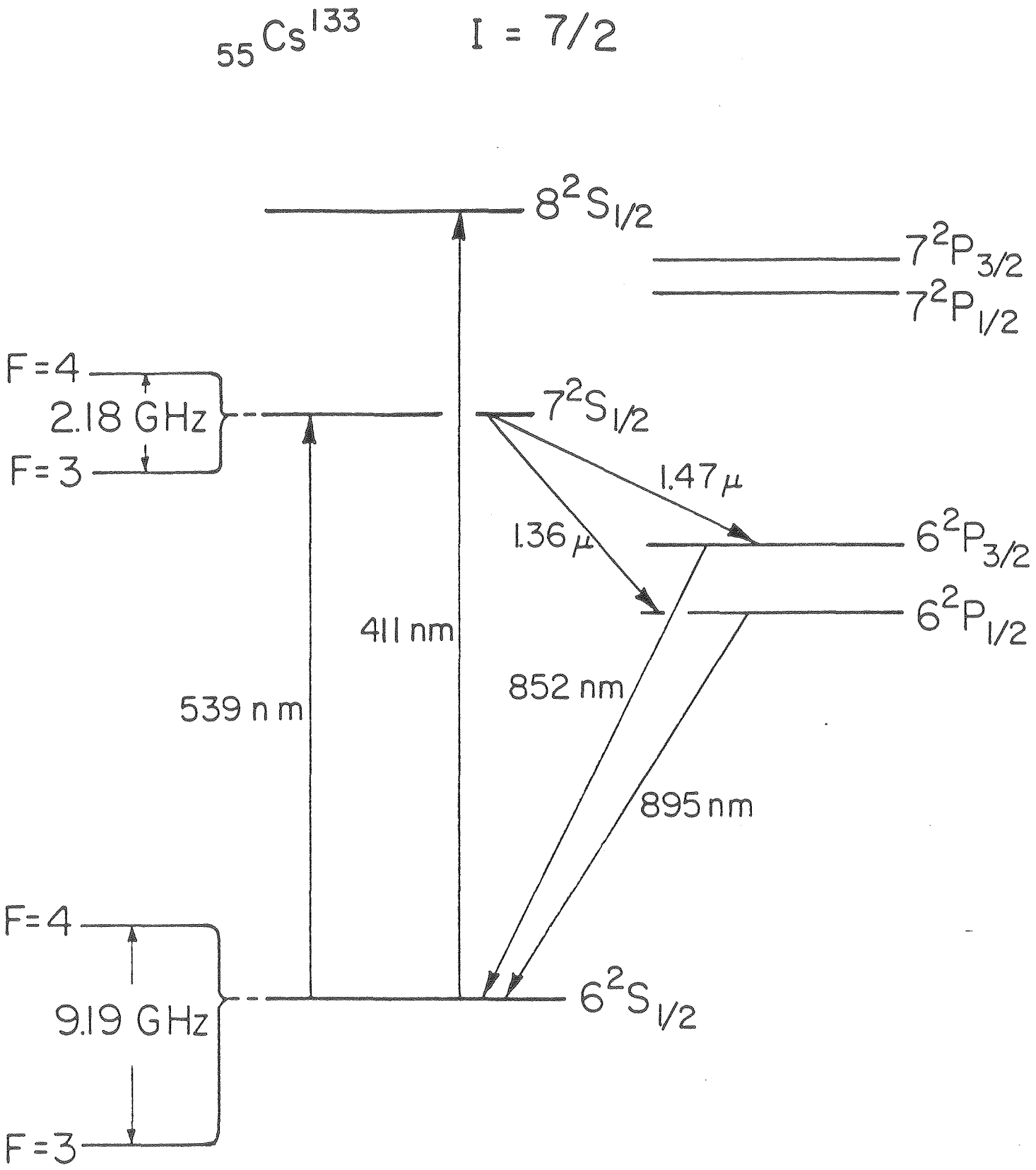


Figure 12

XBL801-4576

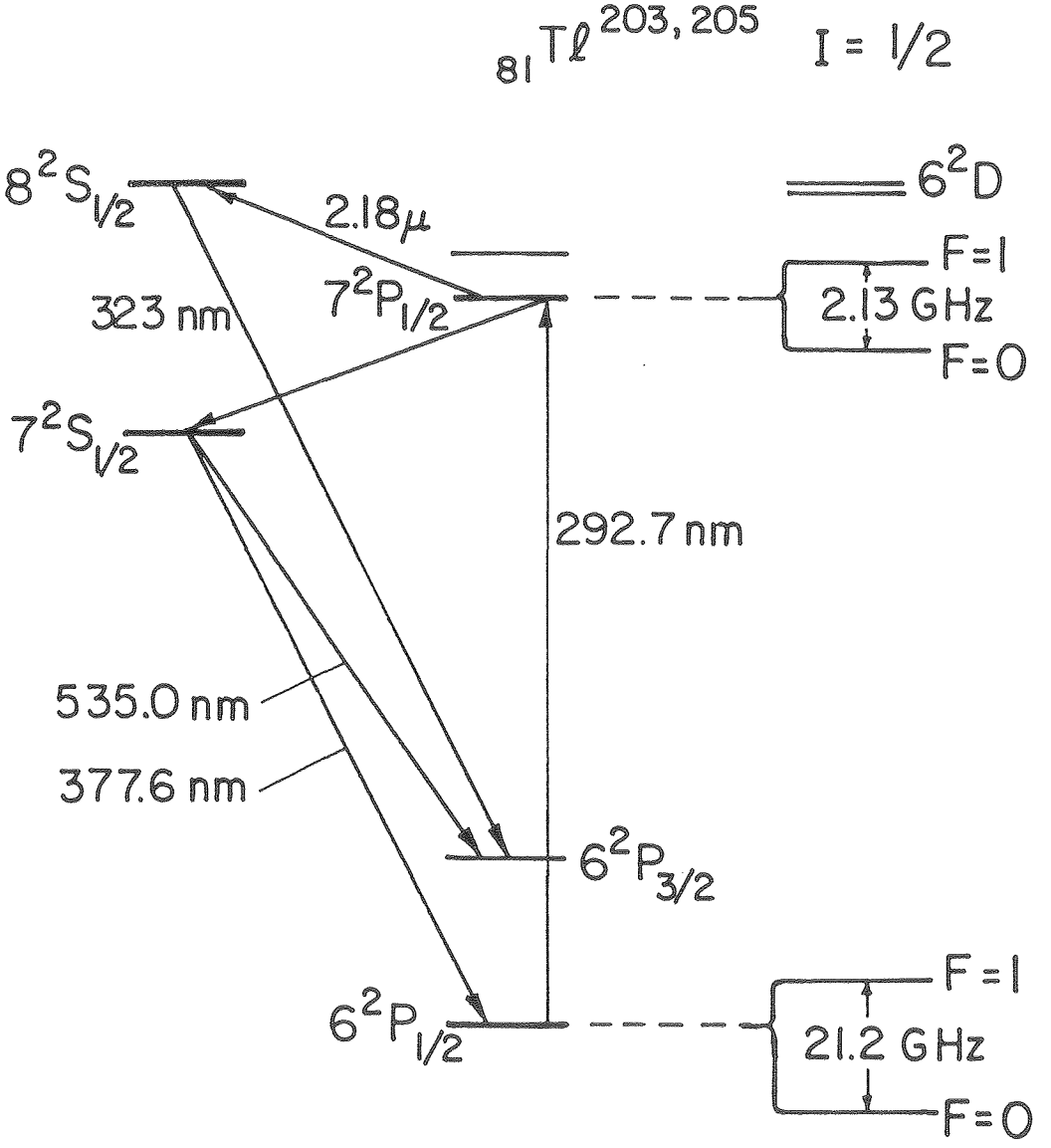
$_{81}Tl^{203,205}$ I = 1/2
$8^2S_{1/2}$
2.18μ
$6^2D$
F=1
323 nm
$7^2P_{1/2}$
2.13 GHz
F=0
$7^2S_{1/2}$
292.7 nm
535.0 nm
377.6 nm
$6^2P_{3/2}$
F=1
$6^2P_{1/2}$
21.2 GHz
F=0
XBL 801-4574

Figure
13

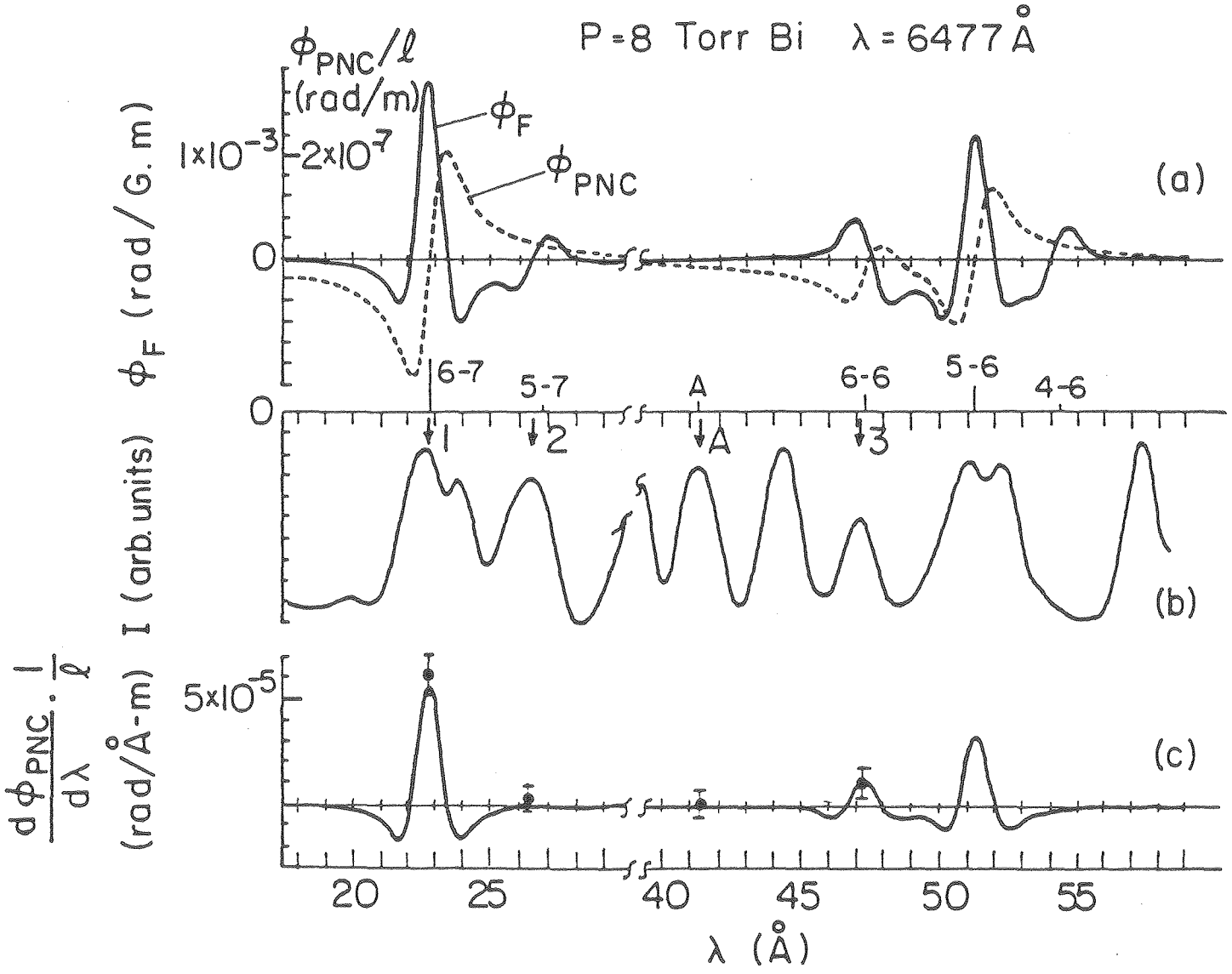
P=8 Torr Bi λ = 6477 Å
$\phi_{PNC}/\ell$
(rad/m)
$\phi_F$
$\phi_{PNC}$
1×10⁻³
2×10⁻⁷
0
(a)
6-7
5-7
A
6-6
5-6
4-6
1
2
A
3
(b)
$\frac{d\phi_{PNC}}{d\lambda}\cdot\frac{1}{\ell}$
(rad/Å-m)
I (arb. units)
$\phi_F$ (rad/G.m)
5×10⁻⁵
(c)
20
25
40
45
50
55
λ (Å)
XBL801-4575

Figure
14

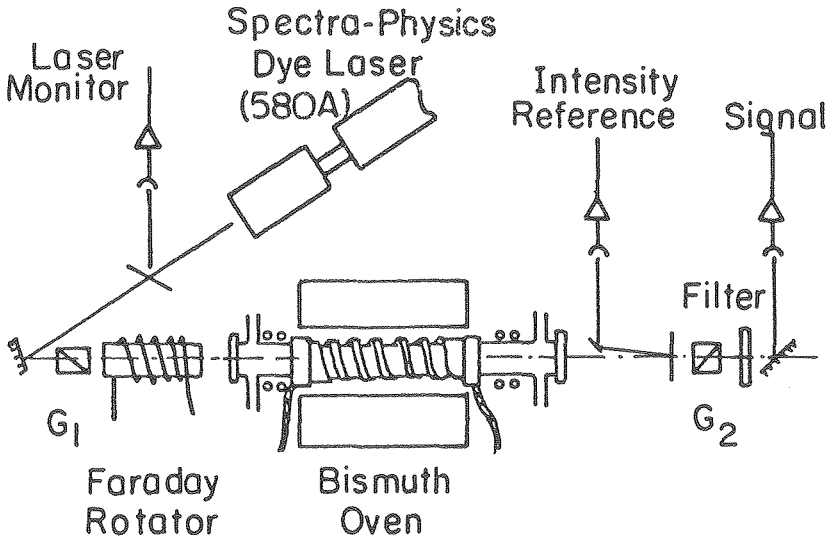


a) OXFORD

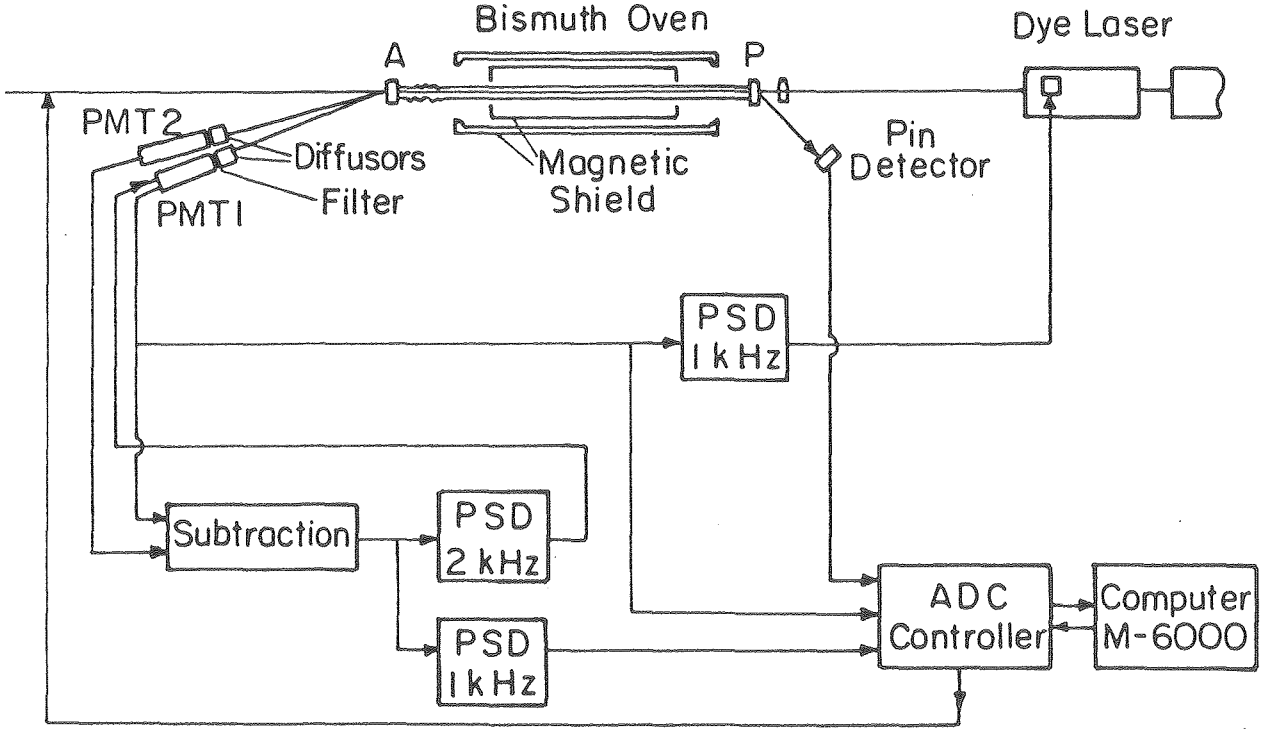


b) NOVOSIBIRSK

Figure
15

XBL 801-4578

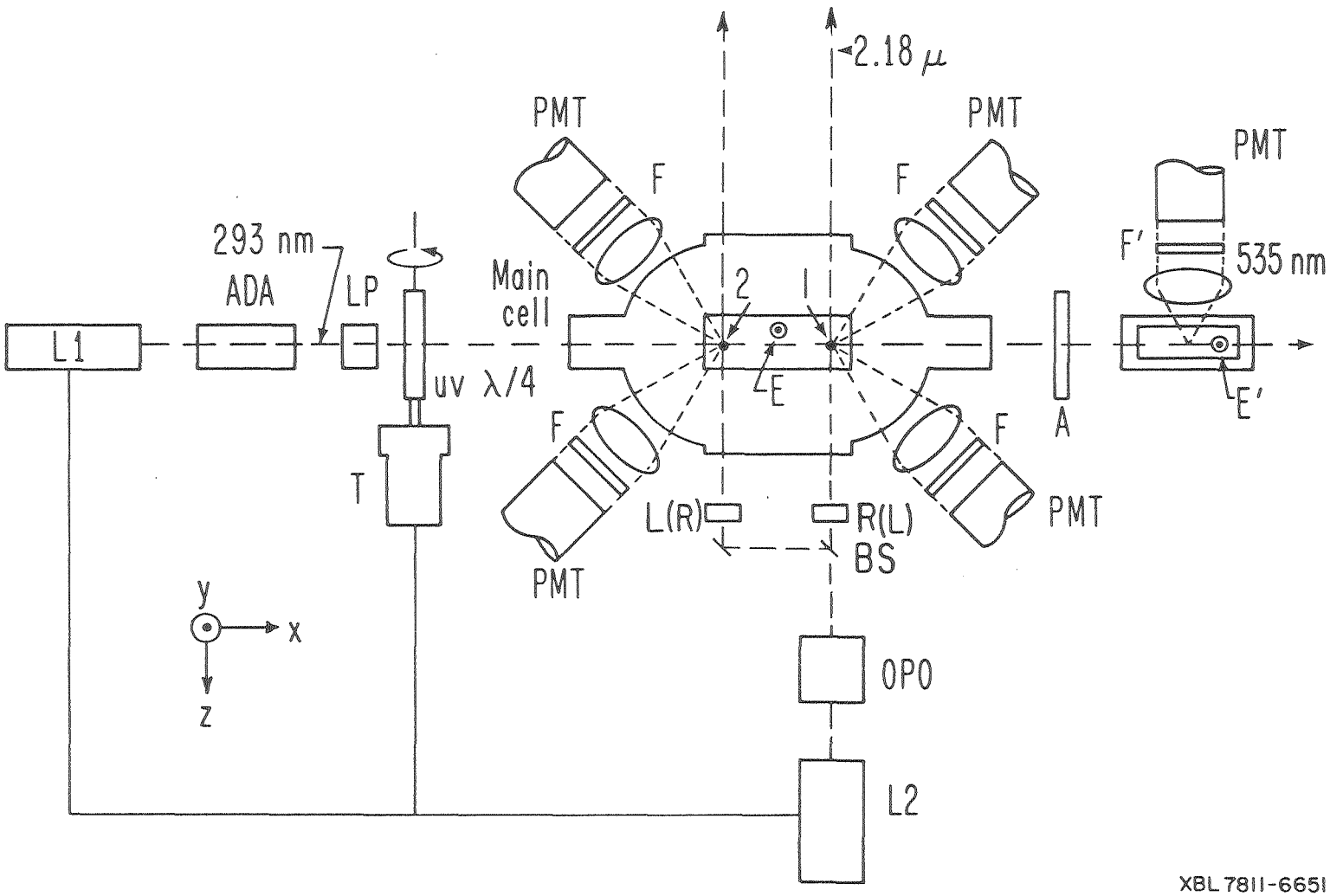
2.18 μ
PMT
PMT
PMT
F
F
F'
535 nm
293 nm
ADA
LP
Main
cell
2
1
L1
uv λ/4
E
E'
A
F
F
T
L(R)
R(L)
BS
PMT
PMT
y
x
z
OPO
L2
XBL 7811-6651A

Figure
16

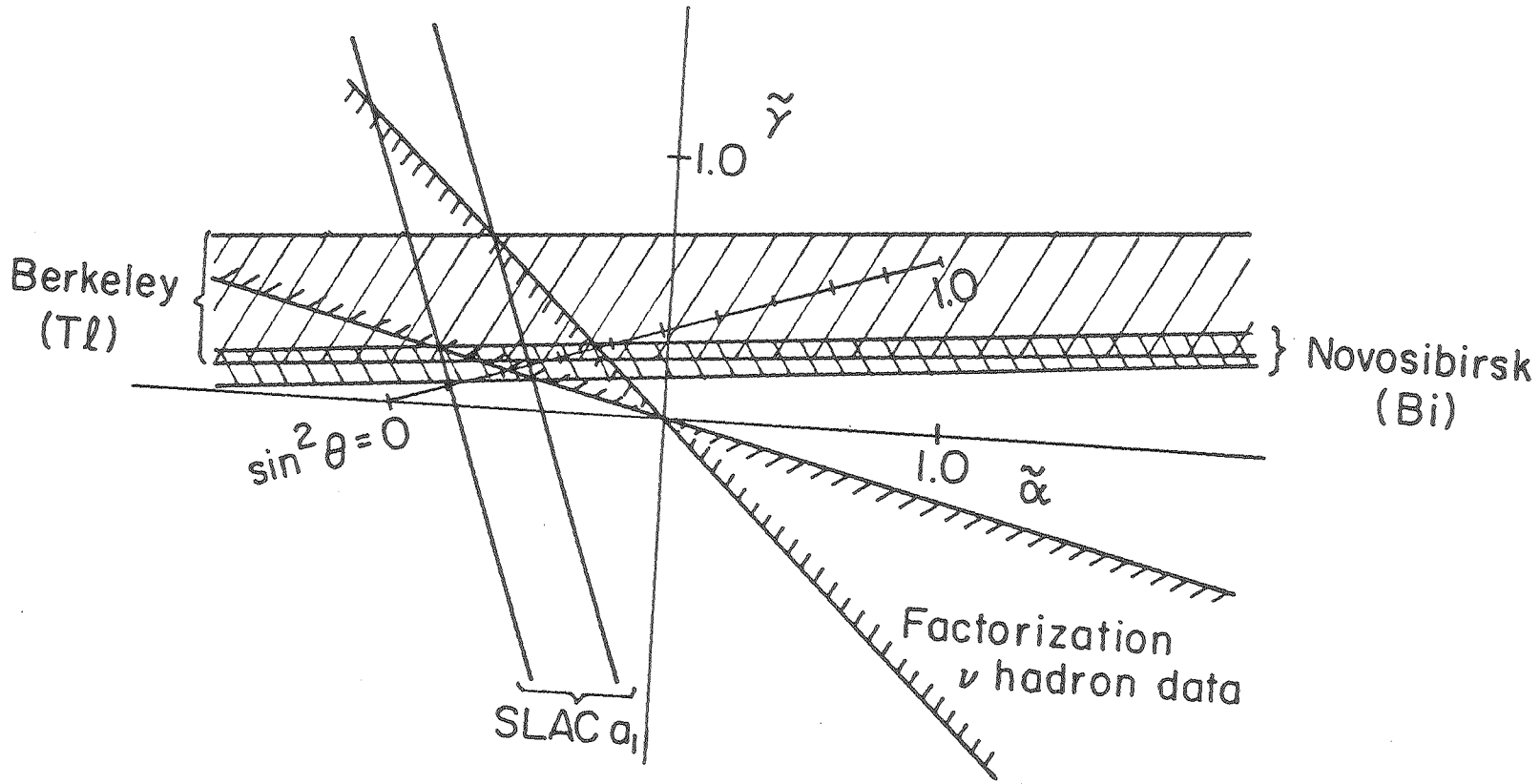


Figure
17

XBL801-4581